ANL/ESD/12-15

Geothermal Life-Cycle Assessment – Part 3

Energy Systems Division

ANL/ESD/12-15

Geothermal Life-Cycle Assessment – Part 3

by
J.L. Sullivan, E. Frank, J. Han, A. Elgowainy, and M.Q. Wang
Energy Systems Division, Argonne National Laboratory

November 1, 2012

CONTENTS

FIGURES

FIGURES (Cont.)

TABLES

TABLES (Cont.)

ACKNOWLEDGEMENTS

The Geothermal Technologies Program in the U.S. Department of Energy's Office of Energy Efficiency and Renewable Energy sponsored this work. Argonne National Laboratory is a DOE laboratory managed by UChicago Argonne, LLC, under Contract No. DE-AC02-06CH11357. We are grateful to Arlene Anderson of the Geothermal Technologies Program for her guidance and input.

Geothermal Life-Cycle Assessment – Part 3

J.L. Sullivan, E. Frank, J. Han, A. Elgowainy, and M.Q. Wang

ABSTRACT

A set of key issues pertaining to the environmental performance of geothermal electric power have been addressed. They include: (1) greenhouse gas (GHG) emissions from geothermal facilities, (2) the use of supercritical carbon dioxide ($scCO_2$) as a geofluid for enhanced geothermal systems (EGS), (3) quantifying the impact of well-field exploration on the life cycle of geothermal power, and (4) criteria pollutant emissions for geothermal and other electric power generation. A GHG emission rate (g/kWh) distribution as a function of cumulative running capacity for California is presented for conventional geothermal steam plants based on data from the California state government and the U.S. government. The distribution is similar to the published global distribution for the same technology. Also presented is a model which was developed to estimate the life-cycle energy of and CO_2 emissions from a coupled pair of coal and EGS plants, the latter of which is powered by $scCO_2$ captured from the coal plant. Depending on the CO_2 capture rate on the coal side and the CO_2 consumption rate on the EGS side, significant reductions in GHG emissions were computed when the coupled system was compared to a conventional stand-alone coal plant. The accumulation of atmospheric CO_2 emissions from the coupled system, prompt on the coal side and from reservoir leakage on the EGS side, was included in the analysis, as well as the subsequent decline of these emissions after entering the atmosphere over a timeframe of 100 years. For this hypothetical system, EGS $scCO_2$ consumption acts as a sequestration mechanism for the coal plant. We also present a model for providing better estimates of the impact of well-field exploration on the life-cycle performance of geothermal power production. The new estimates increase the overall life-cycle metrics for the geothermal systems over those previously estimated. Finally, updated criteria pollutant emission results are discussed for a range of renewable (including geothermal) and other power-generating technologies. These results have been integrated into the Greenhouse Gases, Regulated Emissions and Energy in Transportation (GREET) model.

This page intentionally blank.

1 INTRODUCTION

Reliable and affordable electric power provides invaluable support for the standard of living in the United States, and its ready availability is a key enabler of the U.S. industrial and commercial sectors. About 40% of our primary energy consumption is devoted to generating electric power and most of it is derived from fossil resources [EIA, 2010]. However, concern over climate change and energy security has prompted a reevaluation of primary energy consumption in the United States, especially from fossil resources. In efforts to reduce fossil fuel consumption, some states have already adopted "Renewable Portfolio Standards" and hence, are adding more wind, solar, and others types of renewable energy to their sets of generating technologies. The Energy Information Administration (EIA) [2010] projects that renewable electricity, which now represents about 8.5% of U.S. electricity generation, will increase to about 17% by 2035. Most of this increase is projected to come from additional wind turbines and biomass combustion plants. However, geothermal electricity generation is another renewable generating technology that can significantly enable reductions in fossil fuel consumption. It is expected to grow somewhat over the next decade or two, perhaps significantly if widespread deployment of enhanced geothermal systems (EGS) is realized. This technology is anticipated to operate on the more broadly available, lower-temperature geofluids.

This report is the fifth in a series of life-cycle assessment (LCA) reports [Sullivan et al., 2010, 2011 and Clark et al., 2010, 2011] on geothermal power and its comparison to other power production technologies. The other power production technologies included coal boiler and integrated gasification combined cycle (IGCC); natural gas combined cycle (NGCC); pressurized and boiling water nuclear reactors (N-PWR and N-BWR) for conventional thermoelectric facilities. Representing renewable technologies were hydroelectric; photovoltaic (PV); wind; biomass combustion boiler and IGCC; and concentrated solar power (CSP). Also included in the renewable electricity sources were geothermal technologies such as hydrothermal flash (HT-F), hydrothermal binary (HT-B), EGS, and two variants of geo-pressured gas and electric from reworked (GPGE-rw) and green field sites (GPGE-gf). GPGE and CSP plants are termed hybrid facilities. The former co-produces fossil (gas) and renewable energy (geothermal electricity) and the latter either coproduces solar and gas power (assumed here to be a combined cycle turbine) or uses natural gas for auxiliary purposes during operation. The LCA in these reports quantifies for the various power generating technologies their fuel and plant cycles, where the latter is an itemization of the materials and energy needed for power plant construction. From the earlier reports, key conclusions per kWh of electricity delivered include: (1) fossil plants have by far the greatest life-cycle greenhouse gas emissions (GHGs) of all the technologies; (2) of the renewable technologies, biomass combustion, HT-F, and GPGE have the highest GHGs; (3) conventional thermoelectric plants (coal, natural gas, nuclear, and biomass combustion) require the least materials; (4) renewable power technologies require more materials, especially hydroelectric, EGS; (5) of all materials, cement/concrete and steel are used to the greatest extent across all generation technologies except for PV; and (6) GHG emissions from the plant cycle are greatest for the renewable power technologies, with PV and EGS having the most. Most of these results have already been incorporated into Argonne's "Greenhouse Gases, Regulated Emissions and Energy in Transportation – GREET" model [GREET1, 2012; Wang, et al., 1999].

Despite the work already completed on the life-cycle performance of geothermal power, tasks remain to be completed. For example, the life-cycle performance of geothermal power is affected by GHGs emitted during power production, and by exploration activities during plant- and well-field development. The latter can potentially have a significant impact on well-field development. Supercritical carbon dioxide ($scCO_2$) has been proposed as a substitute for brine geofluids used in EGS systems for purposes of greater energy extraction in some cases or when inadequate water resources are available for conventional EGS. The life-cycle implications of this approach have not been elucidated to date. Another important set of life-cycle metrics is to determine criteria pollutant emission rates (g/kWh) from geothermal and other power plants. GREET computes fossil, petroleum, and total energy use (including renewable energy in biomass); emissions of GHGs (CO_2, CH_4, and N_2O); and emissions of six combustion pollutants: carbon monoxide (CO), volatile organic compounds (VOCs), nitrogen oxides (NO_x), sulfur oxides (SO_x), particulate matter with a diameter below 10 micrometers (PM_{10}), and particulate matter with a diameter below 2.5 micrometers ($PM_{2.5}$). GREET includes electrical power generation from fossil fuels, nuclear fuels, and renewable energy sources including solar and geothermal power production with hydrothermal and water-EGS technologies.

The purpose of this report is to present our results and findings in the areas cited above. More specifically, the status of our assessment of the distribution of GHG emissions from U.S. geothermal power plants is presented with recommendations for acquiring improved data. Also given are LCA modeling results on the use of $scCO_2$ derived from fossil plants in EGS scenarios and its impact on carbon sequestration. In addition, a model is presented which has been developed to estimate the impact of well-field exploration on the LCA of geothermal facilities. Finally, results are presented on criteria pollutant emissions for the various power generation technologies including geothermal power. Those results have been integrated into the GREET model.

2 METHOD

The methodology used herein is the same as previously discussed [Sullivan et al., 2010, 2011]. The life-cycle calculations presented herein are based on process life-cycle assessments, often referred to as process chain analyses (PCAs). This approach strictly employs detailed process-specific data that (ideally) are fully speciated in terms of purchased energy units (e.g., liters [L], kilowatt-hours [kWh], cubic meters [m^3], kilograms [kg], tonnes), specific materials consumption levels (e.g., tons, kilograms, tonnes), and emissions (e.g., grams, kilograms, other). If such values for energy are not available, megajoule (MJ) or British thermal unit (Btu) values are acceptable, although these are less desirable due to ambiguities on whether they represent high- or low-heat values and on whether they are life-cycle or purchased-energy values. All energy values employed herein are low-heat values (LHV).

The system boundary for our study is depicted in Figure 1; the product is the lifetime of kilowatt-hours of electricity at the wall outlet, unless stated otherwise. As Figure 1 shows, the life-cycle stages covered are the fuel-cycle and plant-cycle stages. The former includes fuel production and fuel use during plant operation and the latter consists of onsite plant construction activities and the production of materials comprising plant structures and equipment. Because plant decommissioning and recycling stages are expected to be only a fraction of plant cycle burdens, which in turn are at most marginal in magnitude, they are not considered here.

For the plant cycle stage, the materials tracked were concrete, steel, aluminum, copper, glass, silicon, iron, and plastics which are needed for making plant buildings, wells, enclosures, and equipment (e.g., turbines, generators, heat exchangers). Also tracked for each scenario were plant performance characteristics, such as capacity, capacity factor, and lifetime. Determined

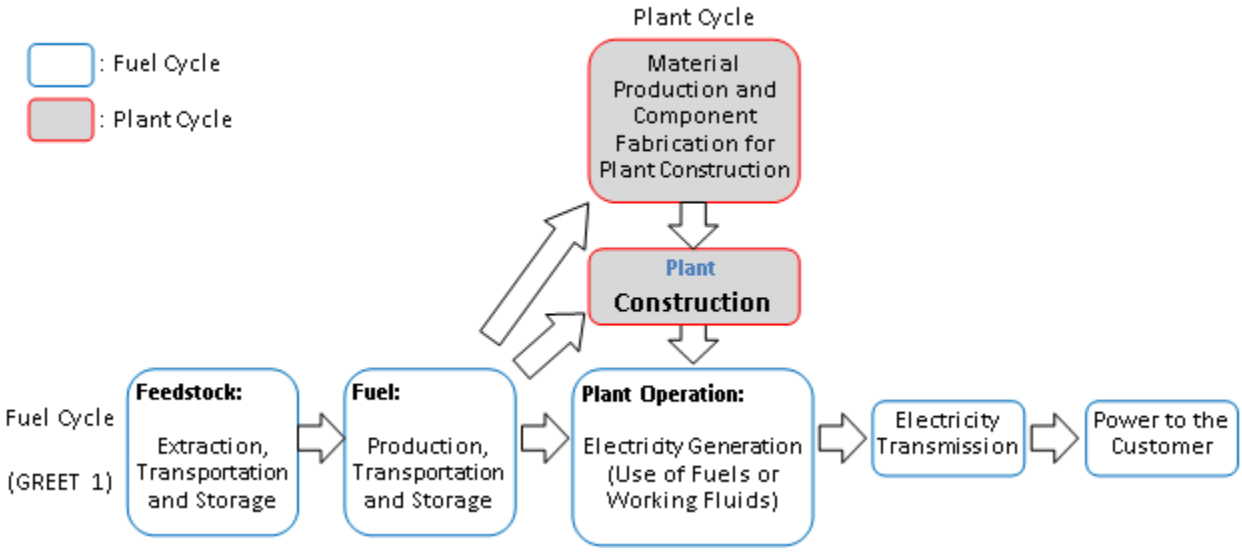

FIGURE 1 System Boundary for GREET Electricity Modules

material compositional data were normalized on a per-megawatt (MW) output capacity and are henceforth termed material-to-power ratios (MPRs). For solid materials, the units are tonnes (metric tons – mt) per megawatt of output capacity; in the case of liquids, the units are kiloliters (kL) per MW. In the few cases where energy units were cited, the same term was used. The MPRs can be thought of as metrics based on a "hardware functional unit" (i.e., a megawatt of output capacity).

MPRs were straightforwardly computed on the basis of facility material requirements divided by plant output capacity. In the case of EGS, HT-B, and HT-F, capacity is based on a single output (i.e., MW of electric power – MW_{el}). On the other hand, for GPGE there are two energy output flows: electric power (MW_{el}) and a natural gas production rate (MW_{th}). The sum of the two is the facility output capacity (i.e., megawatt mixed – MW_{mx}). In cases where natural gas produced from GPGE facilities is burned on site to produce electricity, the output is solely electricity (i.e., MW_{el}).

Combining MPRs with plant capacity, lifetime, capacity factor, fuel use, and emissions incurred during the production of plant constituent materials yields two important service functional units for the plant-cycle stage. They are the energy ratio ($\boldsymbol{\mathcal{E}}_{pc} = E_{pc}/E_{out}$) and the CO_2-equivalent specific GHG emissions metric ($GHG_{pc} = \Sigma GHG_i/E_{out}$), where E_{pc} and E_{out} are the plant-cycle energy use and total plant lifetime electricity delivered, respectively. The latter metric is a sum over a number of GHGs in terms of their CO_2-equivalent emissions (GHG_j). In addition to CO_2, the ones of most significance here are methane (CH_4) and nitrous oxide (N_2O). Values of $\boldsymbol{\mathcal{E}}_{pc}$ and GHG_{pc} were estimated for the geothermal technologies and subsequently compared to other renewable and fossil technologies. After that, we compared overall fossil energy consumption and GHG emissions among the technologies (i.e., $\boldsymbol{\mathcal{E}}_{tot}$ and GHG_{tot}, where the subscript "tot" denotes total across both plant and fuel cycles).

3 GHG EMISSION FROM U.S. GEOTHERMAL FACILITIES

The purpose of this section is to quantify GHG emissions from U.S. geothermal facilities. These emissions arise when the geofluids of geothermal power plants get exposed to the atmosphere. For binary plants, there are no GHG emissions, unless extracted geofluids become exposed to the atmosphere. In fact, it is widely assumed [Bloomfield et al., 2003; DiPippo, 1999] that binary plant geofluids are not exposed to the atmosphere and hence emit no GHGs. On the other hand, because such exposure does occur for flash and steam plants, those facilities incur at least some GHG emissions, ranging from just a few grams per kilowatt-hour to values comparable to or even greater than those emitted from a combined cycle natural gas power plant, (i.e., about 530 g/kWh at the plant gate) [GREET1_2012]. Examples of this from global and offshore studies follow.

While we have hearsay evidence that some binary plants redirect some of their geofluids for cooling purposes, resulting in some of the fluid not being returned to the resource, we assumed these uses are atypical and consequently binary plants were treated as non-emitters. However, this topic should be explored further in future research. Hence, due to maturity and availability of relevant information the discussion that follows pertains solely to flash and steam technologies, henceforth denoted as conventional steam plants.

Bloomfield et al. [2003] reported a weighted average emission rate of 91 g/kWh for CO_2 from U.S. geothermal power plants. When considering the other GHG emission cited for these plants, namely methane, the total GHG emission rate becomes 110 g/kWh. Further, because their capacity weighted average included the zero emissions from binary plants, another adjustment is required, since they assumed no GHG emissions from binary plants. Adjusting their average to extract the 14% binary capacity surveyed, the new average GHG emission rate becomes 131 g/kWh (106 g/kWh for CO_2 only). This average represents GHG emissions from only conventional steam plants. Unfortunately, the range of U.S. geothermal emissions rates was not given [Bloomfield, 2003]. Their results were based on a study wherein, by agreement with geothermal plant operators, individual sources and values for provided emission rates remain confidential.

A comprehensive global survey of CO_2 emissions from global operation of geothermal power plants was conducted by Bertani & Thain [2001]. Other GHGs were not included. Their generation emission rate data ranged from 4 to 740 g/kWh and was obtained from 85 conventional steam plants, representing 85% of global capacity. The corresponding weighted average for the global distribution is 122 g/kWh. A similar range of CO_2 emissions, from 30 to 570 g/kWh with an average of 80 g/kWh, has also been reported for plants operating in New Zealand [Rule et al., 2009]. The actual distribution was not reported. While the global average emission rate is reasonably consistent with our adjusted weighted average of the Bloomfield [2003] data (i.e., 106 g/kWh for CO_2 only), we cannot conclude anything about the U.S. GHG emission distribution. However, it is important to determine this emission distribution; the maximum global value just cited is about 40% more than the 528 g/kWh fuel cycle emissions for a NGCC plant operating at 49% efficiency.

The only publicly available information on GHG distributions from U.S. geothermal plants is provided by the California Environmental Protection Agency's Air Resources Board (CARB). Other states with geothermal facilities neither require nor routinely collect GHG emissions from such plants within their jurisdictions. Using the CARB GHG emissions data [CEPA, 2010] and electricity production data from those plants [EIA-923, 2010], we developed emission rates that were subsequently associated with the "running capacities" [GEA, 2012] of the corresponding plants. From a ranked list of emission rates compared with cumulative running capacity, an emission rate distribution curve was developed.

Figure 2 displays GHG emissions as a function of the fraction of cumulative running capacity from geothermal plants both worldwide [Bertani and Thain, 2001] and those for California (CA). The two trends appear quite similar, which suggests that they might be representative of conventional steam geothermal technologies and associated brines/steam. The global values shown in Figure 2 are data from 85 plants aggregated into 50 g/kWh bins, ranging from 0 to 50 to over 500 g/kWh. The California geothermal emissions, on the other hand, arise from 13 individual values reported to CARB, some of which are aggregated values representing several plants and some of which represent single plants. The California data correspond to values from 1,523 MW of running capacity for flash, double flash, and steam plants, which is roughly a quarter of the global capacity (6,800 MW) surveyed by Bertani and Thain [2001]. The "CA" distribution shown in Figure 2 ranges from 11 to 370 g/kWh with a weighted average emission rate of 97.9 g/kWh. Although this value is not much lower than the adjusted

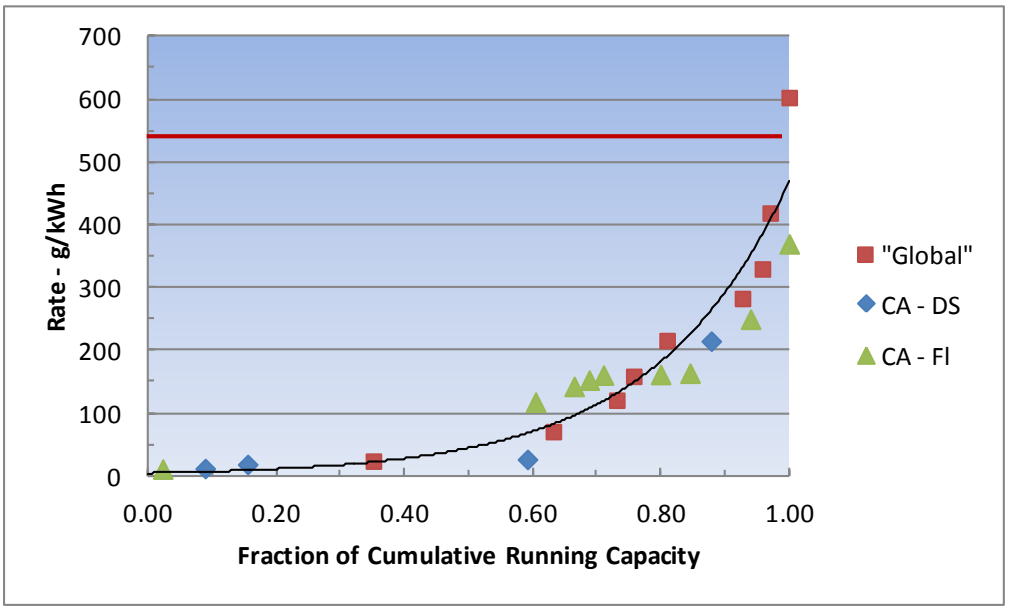

FIGURE 2 Operational CO_2 emissions per generated kWh from flash (Fl) and dry steam (DS) geothermal plants as a function of the fraction of considered plant running capacity for global and California production [CEPA, 2010]. The horizontal red line represents fuel cycle emissions at the plant gate from a natural gas combined cycle plant [GREET1, 2012].

Bloomfield et al. [2003] average value, it does suggest that the California GHG emissions distribution for conventional steam might be different from the Bloomfield's, which covered

more states than just California. On average, dry steam plants shown in Figure 2 appear to have lower GHG emissions than flash plants, but this appearance might be due to a limited number of individual plant data.

Based on the EIA data [EIA-923, 2010], California produces 83% of all U.S. geothermal electricity, and 93% of U.S. geothermal power from conventional steam plants. However, California geothermal GHG emissions are not representative of those from geothermal power production in other states. Only 6% of California's geothermal running capacity is derived from binary plants, whereas this capacity is 63% for Nevada, 25% for Utah, and 100% for Hawaii and Idaho [GEA, 2012]. This is not surprising. California's geothermal power is derived from high-temperature resources that are most efficiently employed using flash plants, whereas geothermal plants in other states typically produce fluids with temperatures more appropriate for binary plants.

The California emission rate distribution curve shown in Figure 2 was developed using actual electricity production values [EIA-923, 2010]. Despite its similarity to the global curve, our estimate of this curve must be considered provisional. First, there is no reason that the two distributions should be in total agreement, due to expected site to site variation in brine composition including dissolved CO_2. More significantly, there are limitations to existing California data that arise primarily from plant emission reporting requirements including the following: not all plants report (due to 2,500 metric tonne reporting threshold); not all plants report all GHGs (CO_2 and CH_4); there are a limited number of facility data points; and finally, an unknown number of plants use a one-size-fits-all emissions factor for their reported values instead of using measured values. This emissions factor, 7.53 × 10-3 g/btu heat extracted, corresponds to 25.7 g/kWh$_{heat}$, which when adjusted by an appropriate range of heat rates (5→ 6½ kWh$_{heat}$/kWh$_{elec.}$) varies from 129 to 162 g/kWh$_{elec}$. For this reason and the others just mentioned, the California conventional steam plant trend shown in Figure 2 might not truly represent the actual GHG emissions distribution for its plants.

Fortunately, starting in 2011 data submitted to CARB must be based on actual measured emission values. Once the data starts making its way through the CARB review process, more accurate assessments will become available for California GHG emissions from geothermal power plants.

Even with higher quality GHG data at hand, the data's significance can be called somewhat into question. The sites for most flash and steam geothermal power plants are locations where the resource is manifested at the surface. This includes hot springs, fumaroles, mud pots, steam vents, and geysers. These features demonstrate the presence of a hot resource and suggest that there is already a background level of GHGs naturally being released at those locations. The question at hand pertains to the degree with which power plant activity affects overall emissions (plant plus background) from the area. Further, will the GHG emissions decrease over time, and if so, by how much? Quantitative answers to these questions must await results from future research.

This page intentionally blank.

4 SUPERCRITICAL CO_2 AS A WORKING FLUID

Existing geothermal electricity generation is almost entirely from geothermal resources where water and steam present in hot permeable rock are brought to the surface for power generation, but relatively few geothermal sites have hot rock perfused with water. EGS inject water from nearby sources into dry geological structures and recover hot water to drive turbines, coupled through a secondary fluid with a low boiling point. EGS expands the potential for geothermal power, but adequate water must be available to deploy it [Tester, 2006].

Brown proposed using supercritical carbon dioxide ($scCO_2$) instead of water to recover heat for EGS [Brown, 2000]. Electricity production from fossil fuels, especially from coal, produces CO_2 that could be captured and compressed to $scCO_2$. If this $scCO_2$ were available near a geothermal resource, it might be utilized for power production; moreover, while water loss below ground is a problem, $scCO_2$ consumption below ground provides the benefit of geological carbon storage.

Supercritical CO_2 requires energy to be produced and transported, so although $scCO_2$ EGS is an appealing idea for increasing geothermal power production, there are questions about net energy consumption when all activities ranging from $scCO_2$ production and transportation through power delivery are considered. Our goal here was to examine the energy consumption and emissions incurred when coal-fired electricity is used to produce top-off $scCO_2$ needed to replace CO_2 lost from the reservoir and when that $scCO_2$ is subsequently transported by pipeline to a geothermal site and utilized for power production. The scope of the study includes GHG emissions and energy consumption associated with producing 1 MWh of total electricity before transmission. Activities related to procuring and using fuels (fuel cycle) and activities related to plant construction (plant cycle) are included. The fuel cycle includes the production and transportation of $scCO_2$. A separate discussion of our treatment can be found elsewhere [Frank et al., 2012].

4.1 SYSTEM DESCRIPTION

There are advantages and challenges that result from using $scCO_2$ instead of water for geothermal heat recovery. Supercritical CO_2 has gaslike properties when propagating through rock, and it has a viscosity that is 40% that of water [Brown, 2000]. For certain conditions, these properties enable $scCO_2$ to permeate rock more easily than water. Further, $scCO_2$ density decreases enough when heated below ground that the buoyancy of hot $scCO_2$ can produce a thermal siphon effect that reduces pumping requirements. The low-heat capacity of $scCO_2$ relative to water (roughly 40%) potentially offsets these advantages, but the low viscosity and thermal siphon effect can result in higher circulation rates so that, when considered on the basis of required pumping energy, estimated net heat production for $scCO_2$ is comparable to that of water [Brown, 2000]. Finally, in areas where water rights are an issue, substituting $scCO_2$ for water might represent an important advantage.

The $scCO_2$ consumption (storage) rate affects the system concept. Some researchers estimate $scCO_2$ consumption from experience with water-EGS. This approach estimates $scCO_2$ consumption to be 5% of the $scCO_2$ flow rate [Pruess and Azaroual, 2006; Pruess, 2007]. In one scenario, each MW of $scCO_2$ EGS power would require 3 MW of coal-fired power to supply adequate $scCO_2$ to meet the $scCO_2$ EGS consumption rate [Pruess, 2007]. If consumption rates were this high, the geothermal system would require an $scCO_2$ pipeline to meet the $scCO_2$ demand. In this scenario, the $scCO_2$ EGS system serves as a sequestration mechanism for the (upstream) fossil-based power plant that, in addition, generates renewable electrical power as a byproduct of the sequestration process.

A contrasting scenario estimates much lower $scCO_2$ consumption [Dunn ,2010; Mobley, 2011]. The scenario considered by these authors utilizes deep impermeable rock as the heat source. There are four mechanisms that can result in the loss of $scCO_2$ from the reservoir: hydrodynamic trapping in pores of a porous rock capped by impermeable rock; solubility trapping in water or other liquids such as crude oil within porous rock; adsorption trapping on organic matter in coal seams and shale; and mineral trapping from reactions with silicates resulting in immobilized carbonates [Nelson et al., 2005]. In the stimulated (fractured) impermeable rock model of Dunn and Mobley, only mineral trapping is possible resulting in low consumption rates [Dunn, 2010]. Incidentally, mineral trapping might reduce fluid flow rates. In one of their scenarios, consumption was only 0.1% of flow. In such a scenario, the $scCO_2$ consumption can be met with a moderately sized on-site generator, no pipeline is required, and almost 75% of the total power output derives from geothermal energy [Mobley, 2011].

4.2 SYSTEM BOUNDARY AND FUNCTIONAL UNIT

The system boundary, depicted in Figure 3, includes coal mining, coal transportation to the power plant, and all operations at the power plant. For the $scCO_2$ EGS, the system boundary also includes CO_2 capture, compression to $scCO_2$, transportation to the $scCO_2$ EGS site, and power production. The activities just described represent the "fuel cycle." Energy and emissions for constructing the power plant infrastructure belong to the "plant cycle" and are also included. The functional unit is 1 kWh of electricity from the combined system, coal, and EGS power facilities. Data from the GREET model were employed for both fuel and plant cycles of the combined system.

The analysis presented in this work focused on the high-consumption scenario, but examined a wide range of $scCO_2$ consumption rates. In the high-consumption scenario, an $scCO_2$ pipeline interconnects a fossil power plant and the $scCO_2$ geothermal power plant. The infrastructure materials for the $scCO_2$ pipeline interconnecting the fossil and $scCO_2$ plants and the energy consumption for its operation are also included.

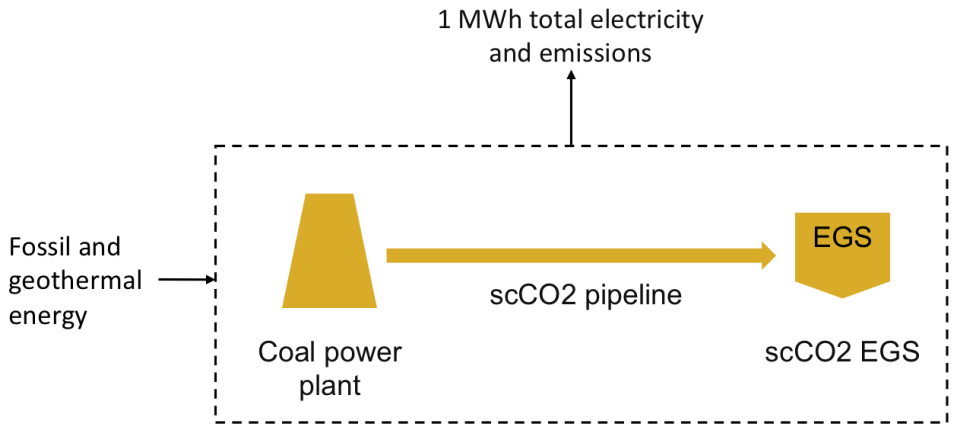

FIGURE 3 System diagram for $scCO_2$ EGS power. A fossil power plant supplies the $scCO_2$ feedstock that is consumed (sequestered) during $scCO_2$ EGS power generation.

4.3 MODEL

The model that follows is a life-cycle assessment tool for estimating high-level energy and emissions of a coupled coal/EGS plant. Some of the CO_2 generated at the coal plant is captured and compressed to a supercritical state and subsequently pumped via pipeline to an EGS plant for extracting heat from the earth. The purpose of this study was to identify and explore the key parameters affecting the life-cycle energy use and GHG emissions associated with producing geothermal electricity when $scCO_2$ is used as the thermal fluid. The technology is immature and theoretical. Therefore, we have used high-level parameters such as CO_2 capture efficiency and $scCO_2$ consumption rate as the study parameters rather than mechanism-level parameters like flow rates, mineralization rates, $scCO_2$ pressure, and depth to describe the $scCO_2$-EGS system operating in a steady state after the reservoir is fully charged. Had we attempted a mechanistic model, many parameters would have been introduced, such as circulation rates and $scCO_2$ density, but these would have little direct bearing on an LCA analysis. Our approach expands the applicability of the study because by articulating the essential parameters from which life-cycle results may be calculated, any particular mechanistic model (perhaps for a specific site) can estimate LCA results by computing the essential parameters described in our study. On the other hand, had we started from a mechanistic model, it would not have been clear how to apply the results to other circumstances, and sensitivity analysis would have been unduly complicated.

4.3.1 Reservoir Development, Size, and Lifetime

Brown [2000] considers a reservoir in Precambrian crystalline rock developed by hydraulic fracturing with $scCO_2$. The pore fluid is dissolved in the $scCO_2$ and removed over a few weeks. We accounted for energy and emissions associated with plant material production, plant construction, well construction, well field stimulation, and plant-to-well piping [Sullivan et al., 2010].

Turaga et al. [2011] modeled thermal drawdown as a function of circulation given the thermal conductivity, density, specific heat capacity, and thermal diffusivity of rock, water, and $scCO_2$ at 200°C. They concluded that circulation rates must be restricted to below 100 kg/s in a reservoir volume of 0.125 km^3 and fracture spacing must be less than 100 m for the reservoir lifetime to reach 30 years. Remoroza et al. [2011] reached similar conclusions regarding drawdown based on a three-dimensional (3-D) simulation. Brown [2000] assumes a 20-year reservoir lifetime and Dunn 2010 assumes 30 years. In this analysis, we assume a 30-year lifetime for both the plant and the field.

4.3.2 Carbon Capture

Ciferno [2006] reviewed amine-based CO_2 capture for retrofits to existing coal power plants. The CO_2 captured (CC) reduces plant CO_2 emissions, but also decreases plant efficiency because heat is diverted from power generation to regeneration of the amine absorber. Hence, plant heat rate (HR), thermal energy required to produce a unit of electricity (BTU/kWh) increases with the capture rate (CR – % CO_2 captured). Table 1 displays the heat rate adjustment factors (AFs) relative to zero carbon capture based on Ciferno for several CRs. They demonstrate substantial increases in the heat rate associated with carbon capture. These factors also reflect parasitic losses to CO_2 compression, 0.12 KWh/kg-CO_2.

Fuel-cycle emissions for power generation with carbon capture are modeled in this study from the emissions for a coal-fired power plant in GREET1 [2012]. It is assumed that carbon capture will require sulfur removal upstream and that particulates will be removed in the overall process. Therefore, PM_{10}, $PM_{2.5}$, and SO_x emissions are set to zero. Energy required for SO_x and particulate control is negligible [Doctor, 2011]. All other fuel-cycle emissions and energy consumptions at each CR are computed by multiplying the 0% carbon capture heat rate value (10,129 BTU/kWh) before transmission for a coal plant [GREET1, 2012] by the heat rate AFs given in Table 1. Total CO_2 generation, the sum of captured and emitted CO_2, at each CR, is determined the same way. Those results are shown in the third and fourth columns of Table 1.

TABLE 1 Summary of amine-based carbon capture in a coal power plant retrofit. The heat rate adjustment factor (AF) is from Ciferno [2006]. The last three columns are computed from the AF and GREET1 2012 as described in the text.

Capture Rate	Adjustment Factor	Emitted CO_2 (g/kWh)	Captured CO_2 (g/kWh)	Effective Heat Rate[a] (BTU/kWh)
90%	1.434	143	1,289	9,613
70%	1.305	391	913	9,708
50%	1.197	598	598	9,803
30%	1.107	774	332	9,912
0%	1.000	999	0	10,129

[a] Per combined coal and EGS power output - see below.

The $scCO_2$ EGS reservoir must be filled before operation, but the emissions for producing the initial $scCO_2$ charge are small, relative to the emissions from producing and delivering the $scCO_2$. We estimate that the effect of neglecting the emissions from filling the reservoir is to underestimate GHG emissions by 1% for the 90% carbon capture efficiency case.

4.3.3 $scCO_2$ Consumption

Brown [2000] used experience from water-EGS field testing at Fenton Hill to predict 3 kg/s of $scCO_2$ consumption for a 10-MW power system (1,080 kg $scCO_2$/MWh), while Pruess [2007] estimates consumption from 5% consumption of 22 kg/s $scCO_2$ flow per megawatt (3,960 kg $scCO_2$/MWh). The average, 2,520 kg $scCO_2$/MWh, is used in this study.

As depicted in Figure 3, our system is a coupled pair of plants, a coal facility and an EGS facility, where the former provides the latter with the $scCO_2$ required for its operation. Hence, the total electricity produced for 1 MWh of EGS power is

$$El_{tot} = Y/CC + 1, \qquad (1)$$

where Y is the $scCO_2$ consumption rate (g/kWh) of the EGS facility. Hence, using the average consumption given above and the CC for 90%, El_{tot} is 2.93 MWh, 1.93 of which is from coal. At this capture rate, 65% of the power comes from coal. For the 30% capture rate, El_{tot} is 8.52 MWh. The effective heat rate of the combined system, in the fifth column of Table 1, is just the fossil heat rate of the CCS coal plant at each capture rate scaled by the corresponding ratio of coal to total system power: $HR(CR) = 10{,}129 \times AF(CR) \times Y/CC/El_{tot}$. The decrease in effective heat with increasing CR seen in the table demonstrates that the power generated by the $scCO_2$ EGS plant using captured CO_2 more than offsets the energy consumed at the coal plant for carbon capture.

4.3.4 Pipeline Requirements

Pipelines for $scCO_2$ delivery require materials for construction (plant cycle LCA) and require power for operation (fuel cycle LCA). Both of these depend on transportation distance. Two references [Dooley et al., 2009; ICF, 2009] discuss pipeline requirements in the United States for carbon capture and sequestration (CCS). Dooley et al. [2009] estimates tens of miles between the source and sink. ICF [2009] considers $scCO_2$ pipeline infrastructure requirements that would be required to meet expected U.S. CO_2 reduction mandates; therefore, the ICF analysis required estimation of pipeline distances to connect CO_2 sources to geological sequestration sites. They estimated an average distance of 50 mi per power plant if a common network infrastructure were built. Given the distance between power plants in the far west, where most geothermal power plants are located, is likely to be larger than this, and we conservatively estimate a distance of 100 km (62 mi). It will be seen that this parameter has little effect on $scCO_2$ EGS LCA.

Supercritical CO_2 pipelines require a API 5L grade of X65 or X70 pipeline carbon steel for dry pumping; otherwise, stainless steel is required when moisture is present. Economic flow velocities range between 1.5 to 2 m/s [Element Energy Limited, 2010]. Typical assumptions of pressures are approximately 15 MPa [ICF, 2009].

Analysis of $scCO_2$ pipeline configurations [ICF, 2009] demonstrated that the pipeline steel use (kg steel/m) per flow of $scCO_2$ (kg $scCO_2$/s) is independent of pipeline diameter. Pipeline steel use increases with pipeline diameter, but so does pipeline flow, and the two effects cancel one another. Therefore, if steel is the primary infrastructure material for the pipeline, then the pipeline configuration details will not affect the present analysis. The pipeline configurations in ICF [2009] required 0.74 kg steel/m for each kg/s of $scCO_2$ flow when the $scCO_2$ velocity was 1.5 m/s. For example, a 16-in. outside diameter trunk pipeline (0.42-in. wall thickness) uses 104 kg steel/m and, when operating with 1.5 m/s velocity flow across its 0.385 m inside diameter, transports 140 kg $scCO_2$/s, which would support 200 MW of $scCO_2$ power generation consuming 2,520 kg $scCO_2$/MWh.

Gurgenci et al. [2009] comment that the pipeline, transmission lines, and power generation plant must be relocated every 15 years (presumably because of thermal draw-down). Assuming each deployment shifts the system 5 km, then the pipeline requirements will be the main trunk (100 km) amortized over the carbon flow accrued over the assumed 30-year lifetime, plus an additional 5 km of pipeline every 15 years. We neglect this additional 5 km.

4.3.5 Pipeline Pumping

Pumping power is tabulated in ICF [2009] for several scenarios corresponding to several sequestered masses. If these powers support the average 50-mi transport distance studied in ICF [2009], then the average pumping power from that reference is 3.83×10^{-5} KWh/kg/km. The default value in GREET1 2012 is 3.18×10^{-5} KWh/kg/km. Using the default value, our assumed $scCO_2$ consumption rate, and a 100-km pipeline, the pumping power is about 8 kWh per MWh generated. This is less than 1% of the output power.

4.3.6 $scCO_2$ Infrastructure Materials On Site

Table 2a in Sullivan et al. [2010] displays the material masses used to construct EGS wells and shows the materials for surface piping between well and plant. The surface piping is only 1.7%, 4.1%, and 1.7% of the cement, diesel, and steel, respectively, for well construction. Therefore, differences in well spacing between $scCO_2$ and the EGS-50 case in Sullivan et al. will have little effect on the materials analysis for $scCO_2$ compared to water EGS. We make the approximation that the $scCO_2$ well casing diameters and properties are the same for $scCO_2$ EGS wells and for water-EGS wells of equal depth. For these reasons, this analysis uses the infrastructure materials for the EGS-50 case in Sullivan et al. [2010] for the $scCO_2$ case. Energy and emissions from infrastructure materials were extracted from GREET1_2012 for the EGS scenario with 6 km wells with 3 liners. The steel requirements were increased to account for the 100-km $scCO_2$ pipeline. The result is in Table 2. As in other analyses, we neglect infrastructure

TABLE 2 Plant cycle energy use and emissions for power plant infrastructure per unit of power at the plant gate computed by adding 100 km of $scCO_2$ pipeline to values for water EGS in Sullivan [2010]. Despite the 100-km length, the pipeline has minor effects on power plant infrastructure related emissions and energy use.

	water EGS	$scCO_2$ EGS
Energy Use: BTU per MMBTU electricity		
Total energy	59,643	60,588
Fossil fuels	53,072	53,958
Coal	24,365	24,638
Natural gas	15,428	16,028
Petroleum	13,279	13,293
Total Emissions: grams per MMBTU		
VOC	0.830	0.837
CO	7.272	7.291
NO_x	8.740	8.808
PM_{10}	7.437	7.492
$PM_{2.5}$	2.974	2.991
SO_x	12.040	12.128
CH_4	11.919	12.061
N_2O	0.054	0.055
CO_2	6,322	6,381
CO_2 (with C in VOC and CO)	6,336	6,395
GHG	6,651	6,713

materials to connect the $scCO_2$ EGS system to the grid even though it may be remote [Gurgenci, 2009]. While infrastructure related emissions determine the life-cycle emissions for water EGS, it will be seen below that $scCO_2$ EGS emissions are dominated by the fuel cycle at the coal power plant. Therefore, further sensitivity analysis was not considered for the $scCO_2$ EGS infrastructure.

4.4 RESULTS

Figure 4 shows a set of fossil energy consumption curves relevant to the energy performance of our combined system. In Figure 4, total electricity is described by equation (1). The curves for the coal stand-alone (no carbon capture) and CCS coal stand-alone plants, henceforth denoted as coal and CCS plants, respectively, merely reflect their heat rates; the former without and the latter with a dependence on CR. In both of those cases, plant cycle energy is negligible. The most interesting dependence in Figure 4 is shown by curve for the combined CCS and EGS, hereafter denoted as CCS/EGS, which shows a decrease in fossil energy consumption per unit power out. That energy is:

$$E_{fos} = [(HR(CR)/3413 \times (1 + \varepsilon_e) + \mathcal{E}_{coal}) \times Y/CC + \mathcal{E}_{egs}]/(Y/CC + 1), \quad (2)$$

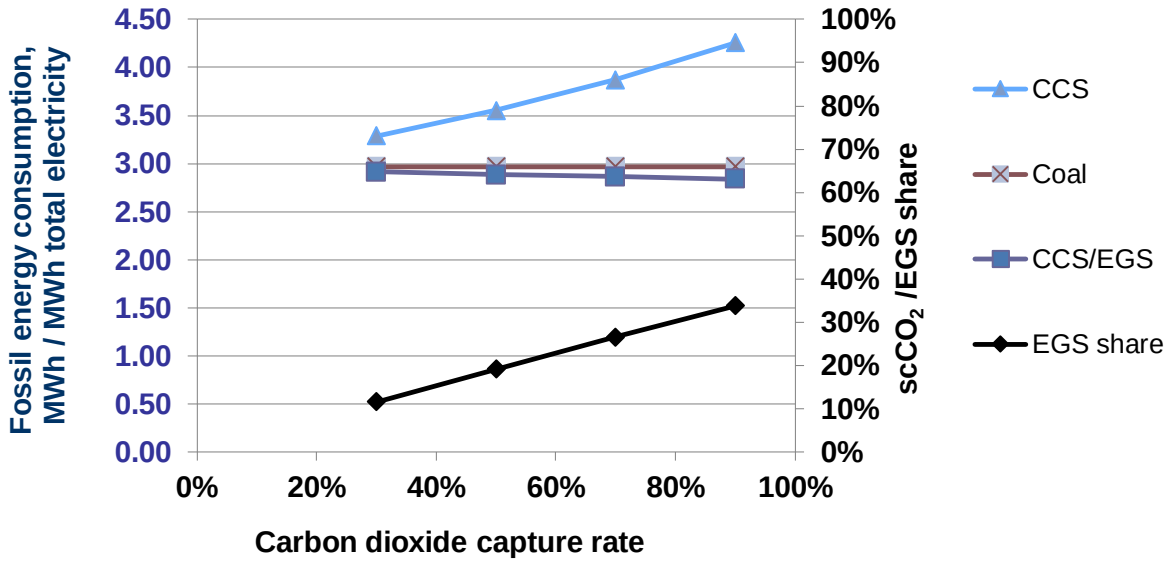

FIGURE 4 Fossil energy consumption and EGS share per total produced electricity at the plant gate for the indicated plants.

where ε_e (0.02 for coal) denotes the ratio of upstream fuel production energy to the fuel use energy, and $\mathcal{E}_{coal}$ and $\mathcal{E}_{egs}$ denote the plant cycle energy ratios at the plant gate for coal and EGS plants. Values of the ratios are 0.0023 and 0.059, respectively. This curve, substantially the CCS coal stand-alone curve adjusted by the ratio of coal to total system power, clearly demonstrates that the combined system uses less fossil energy for all CR per unit power output than the conventional coal plant. Also shown in Figure 4 is the EGS share of the total electricity produced by the CCS/EGS plant, the inverse of equation (1). Note that fossil fuel used for the EGS plant cycle ($\mathcal{E}_{egs}$ = 0.059 MWh/MWh) contributes 2% or less of the total fossil energy use shown in Figure 4 for the CCS/EGS plant, illustrating that infrastructure material related energy use is a minor effect for $scCO_2$ EGS.

Figure 5 shows four GHG emission dependencies on capture rate. The curve for the CCS/EGS plant was determined from the following expression:

$$GHG(CR) = [\varepsilon_c \times (EC + CC) + EC + ghg_{coal}]\ Y/CC + ghg_{egs}]/[Y/CC + 1], \quad (3)$$

where ε_c is the ratio of upstream fuel production GHGs to those for fuel combustion (0.053 – from GREET1 [2012]) and "ghg" terms represent plant cycle emissions. GHG emission values (g/kWh) were obtained from GREET1 [2012] for both fuel and plant cycles and adjusted for CR as per equation (3). For coal plant GHG emissions, equation (3) becomes:

$$GHG(CR) = \varepsilon_c \times (EC + CC) + EC + ghg_{coal}, \quad (4)$$

It is clear from Figure 5 that GHG emissions per MWh decrease with carbon capture for the CCS plant, but even more so for the combined system. This is, of course, due to the leveraging effect

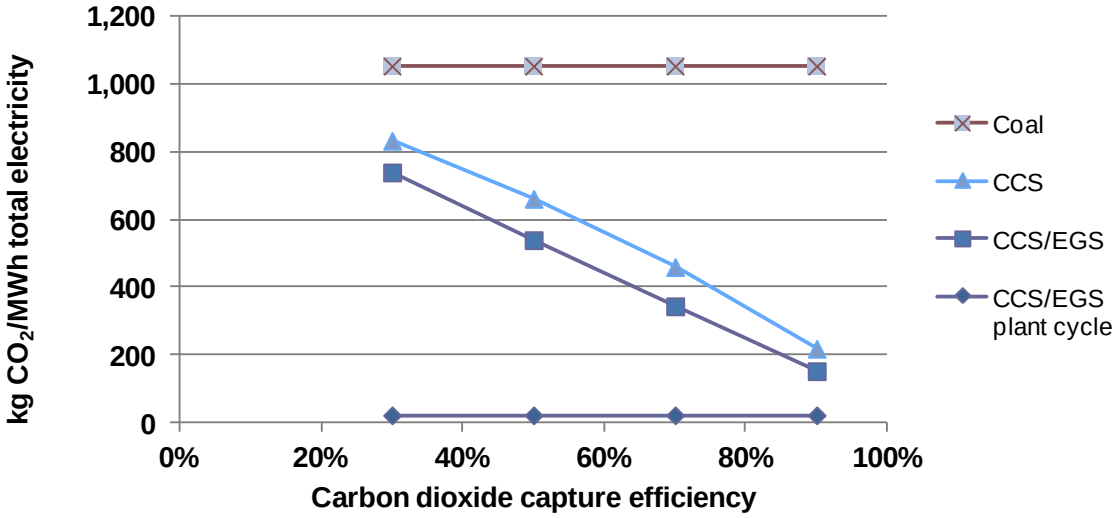

FIGURE 5 GHG emissions before transmission for $scCO_2$ EGS power.

of EGS power. GHG emissions from the coal plant are higher than either of the others. The plant cycle ghg terms in equations (3) and (4) are 0.86 g/kWh for ghg_{coal} and 22.5 for ghg_{egs}, respectively. Figure 5 shows that even for the largest of these two values, ghg_{egs}, plant cycle GHGs make only a minor contribution to the total.

Figure 6 explores the effect of the $scCO_2$ consumption rate on changes in total GHG (ΔGHG) relative to those from a conventional stand alone coal power at a series of CRs. This figure demonstrates that substantial reductions in GHG relative to those from a conventional coal plant can be achieved by coupling a CCS enable coal plant with an $scCO_2$ EGS facility. As expected, lower CR values result in lower GHG reductions.

Reading Figure 6 requires some care because the share of power from geothermal power varies across the abscissa. At low $scCO_2$ consumption, the geothermal plant provides most of the power because the geothermal plant is able to recirculate the $scCO_2$ many times before it is absorbed or lost below ground. Thus, less $scCO_2$ is required from upstream and therefore, less coal-fired power is present in the mix. If the consumption rate is sufficiently low that an onsite power plant can meet the demand, this may help deployment by eliminating the pipeline. At the other extreme, for high consumption rates most of the power comes from the CCS plant and as such the corresponding CO_2 reduction mostly reflects sequestration with a little EGS power in the mix.

Another factor considered for this analysis was leakage of reservoir CO_2 (kg/yr) to the atmosphere. Although there is considerable uncertainty on the magnitude of such a leakage due to the lack of field experience, we nonetheless made the following estimates. We assumed the leakage rate would be dependent on the amount of CO_2 in the ground; a first-order dependence was considered a reasonable approximation. Further, it is important to account for the continual addition of $scCO_2$ to the reservoir during plant operation for every megawatt-hour produced. Hence, our governing rate equation becomes:

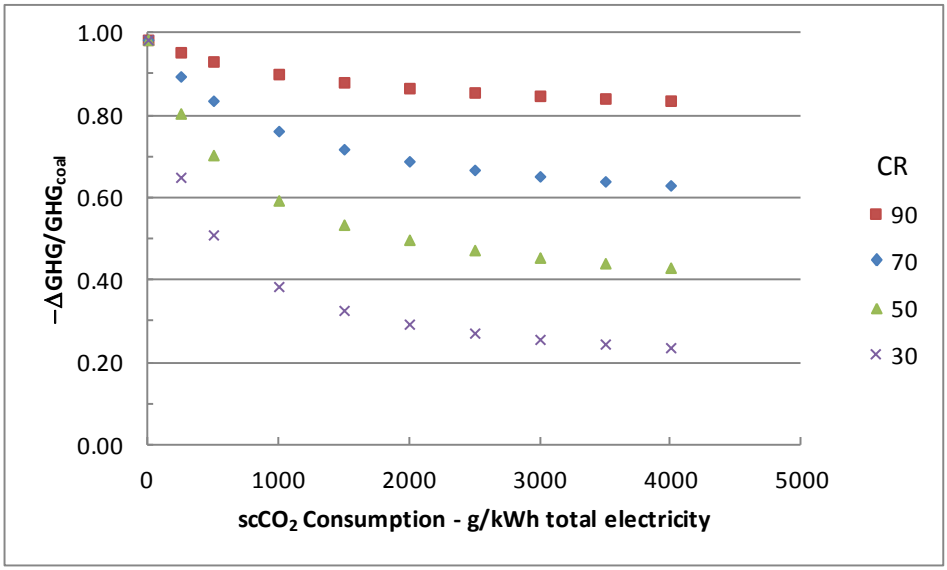

FIGURE 6 Reduction in GHGs vs. $scCO_2$ EGS consumption rates relative to GHG emissions from conventional coal for a CCS/EGS plant at several CO_2 capture rates.

$$dM/_{dt} = -\alpha M(t) + R, \tag{5}$$

where M is the amount of CO_2 in the reservoir, α is the leakage rate (%/yr), and R is the rate of addition of CO_2 to the reservoir, in this case assumed to be 22.08×10^6 kg/yr (2520 kg/MWh × 24 × 365) produced. Solving this equation for two regimes, one for the period during plant operation and the other for post decommissioning, we have:

$$M(t,\alpha) = M_o\, e^{-\alpha t} + R/_{\alpha}\,(1 - e^{-\alpha t}) \tag{6}$$

for t ε (0, LT) and

$$M(t,\alpha) = M(LT)\, e^{-\alpha(t-LT)} \tag{7}$$

for t ε (LT, t'). For these equations, M_o is the initial charge to the reservoir, assumed to be 5 million kg. Reservoir leakage emissions as a function of time are simply computed from EM(t,α) = M(t,0) – M(t,α), where M(t,0) is simply the amount of material present in the reservoir at the starting time, t, for each regime, in this case 0 and LT for equations (6) and (7), respectively.

As already stated, equation (5) is an approximation. Because our treatment of $scCO_2$ EGS power assumes an $scCO_2$ consumption rate, this admits to other loss mechanisms from the reservoir not accounted for, four of which were mentioned above. Hence, results based on equation (5) could be on the higher side.

Based on these expressions and assuming a 90% CR, we estimated the total cumulative CO_2 leaked from the reservoir after 100 years (30 years of operation and 70 years beyond decommissioning of both plants) to be 22 g, 207 g, and 1450 g per kWh of EGS power, for α equal to 0.01%, 0.1%, and 1% per year, respectively. To these emissions we add 219 g/kWh of prompt emissions (life-cycle GHG as per equation (3) and Table 1) from the CCS plant to yield 152 g, 215 g, and 635 g per kWh of combined power , respectively, from the CCS/EGS plant (0.66 kWh from CCS and 0.34 kWh from EGS). Despite greater overall fuel cycle GHGs generated by the combined plant [see Table 2; (CC+EC)*(1+ε_c)] at CR = 90% and taking into account reservoir leakage emissions, the above CCS/EGS plant values are considerably less than prompt fuel cycle emissions of 1,053 g/kWh (equation 4 for CR = 0) from the coal plant.

Over a hundred years, much can happen to the CO_2 emitted to the atmosphere. In fact, there is a redistribution process for CO_2 that is emitted into the atmosphere. This process is known as the carbon cycle, and includes mechanisms whereby CO_2 emitted into the atmosphere is redistributed between the oceans, atmosphere, and biosphere; resulting in a reduction of the added CO_2 in the atmosphere over time. A more complete discussion of this can be found elsewhere [Houghton, 1997]. Various models have been developed to quantify the fate of CO_2 emissions into the atmosphere; one such model is the Bern Carbon Cycle model [Joos et al., 2001]. A detailed discussion of that model is beyond the scope of the present study. Nonetheless, to account for the fate of CO_2 emitted into the atmosphere by our plant and reservoir, we employed a frequently used five-term fit of the computed survival function [Shine et al., 2005; Hansen et al., 2007]:

$$f(t) = \ a_o \ + \ \sum_1^4 a_i \, e^{-t/\tau_i}, \qquad (8)$$

where a_i are dimensionless coefficients and τ_i are decay rates in years. The constants for this expression are: 0.18, 0.14, 0.18, 0.24, and 0.26 for the coefficients of $a_o \ldots a_4$, respectively, and 420, 70, 21, and 3.4 for the decay times of $\tau_1 \ldots \tau_4$, respectively [Shine et al., 2005]. The sum of coefficients is unity. This expression represents model predictions for the fate of a pulse of CO_2 added to the atmosphere. The overall decay rate is very slow. In fact, after 100 years 33% of the original pulse still remains in the atmosphere; 22% remains after 500 years.

To calculate the reductions of the CO_2 added to the atmosphere, the following heredity integral is employed:

$$EM(t) = \ \int_0^t \dot{EM}(s) \ f(t-s)\, ds, \qquad (9)$$

where EM is the remaining CO_2 emissions in the atmosphere, the dotted quantity is the time rate of CO_2 additions, and f(t) is the decay rate (survival function).

Employing equations (5)–(9), we calculated the time dependence of CO_2 emitted into the atmosphere from our CCS/EGS plant. An example plot is shown in Figure 7 for the scenarios specified. The results in the figure represent the sum from two emission sources: those from the CCS plant and those leaking from the EGS scCO_2 reservoir. The latter is operative continuously over time, even after the plant has been decommissioned. A 90% capture rate at the CCS plant

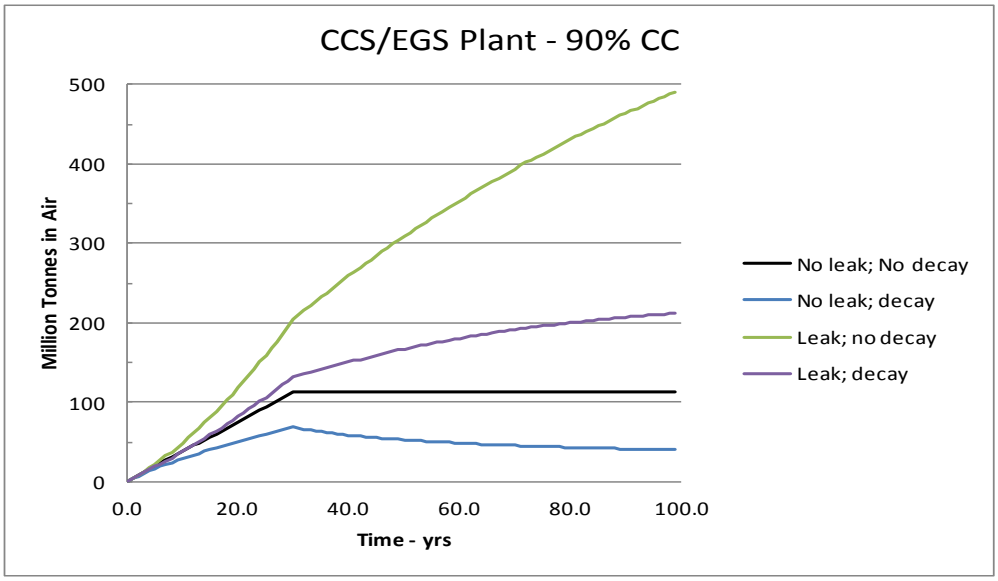

FIGURE 7 CO_2 emissions to the atmosphere over 100 years (30 year plant lifetime) for the CCS/EGS plant and the effect of atmospheric CO_2 attrition on them.

was assumed. For the "no-leak" set, the only emissions are prompt, which are released from the CCS plant. When atmospheric CO_2 decay is added in, there is a significantly lower level of CO_2 remaining in the atmosphere at all times. In fact, at 100 years it is 65% lower.

On the other hand, when reservoir leakage (1%) is added in, the overall emissions levels are almost five times as high as seen upon comparing the "no leak no decay" and the "leak no decay" curves. Again, when atmospheric CO_2 attrition is added in, overall emissions are much lower over all time. It is 57% lower at 100 years.

Significant atmospheric CO_2 attrition is also realized at other leakage rates. After 100 years, we find the remaining atmospheric CO_2 emissions to be 54.5 g, 84.5 g, and 273 g per kWh of CCS/EGS power for α of 0.01%, 0.1%, and 1% respectively. These values are about 60% lower than their "no-decay" counterparts above. Clearly, this is a substantial reduction. Further, even though atmospheric decay is delayed for reservoir CO_2 until it leaks out, the above values are still considerably less than 371 g/kWh remaining after 100 years from the coal plant that had operated for the first 30 years.

4.5 SUMMARY

The purpose of this section was to identify and explore the key parameters affecting the life-cycle energy use and GHG emissions associated with producing geothermal electricity when $scCO_2$ is used as the thermal fluid. The technology is still theoretical and has not yet been demonstrated. Therefore, we have used high-level parameters such as CO_2 capture efficiency of coal power plants and $scCO_2$ consumption rate of geothermal facilities as the study parameters rather than mechanism level parameters such as flow rates, mineralization rates, $scCO_2$ pressure,

and depth to describe the $scCO_2$ EGS system operating in a steady state after the reservoir is fully charged. Had we attempted a mechanistic model, many parameters would have been introduced, such as circulation rates and $scCO_2$ density, which would be speculative at this time; however, they have little *direct* bearing on an LCA analysis. Our approach expands the applicability of the study because by articulating the essential parameters from which life-cycle results may be calculated, any particular mechanistic model, perhaps for a specific site, can estimate LCA results by computing the essential parameters described in our study.

Our first result is that the few parameters introduced here, for example, $scCO_2$ consumption expressed per unit of geothermal electrical energy produced, heat rate for the fossil power source generating the $scCO_2$, and CO_2 capture efficiency, are adequate to support a high-level life-cycle analysis.

The second finding is that the $scCO_2$ geothermal power production must be considered in combination with the upstream $scCO_2$ production since both produce electricity; and thus, both contribute to the electrical-energy based functional unit. The energy consumption and emissions from electricity production associated with top-off $scCO_2$ production account for almost all of the emissions in the combined system. In particular, the emissions associated with plant infrastructure, including pipeline, are small in comparison. Even with 100 km of steel pipeline, the pipeline contributed only 1% of the plant-cycle GHG emissions in Table 2. The 100-km pipeline length assumption, therefore, had little effect on the analysis. Therefore, neglecting pipeline construction for periodic site relocation (Gurgenci [2009], mentioned in Section 3.2.1) will have minimal effect on LCA results.

As analyzed here, and for the assumed 2,520 kg $scCO_2$/MWh, $scCO_2$ EGS acts like an additional power cycle for the associated coal-fired plant. Renewable energy is being used to offset energy losses for CO_2 capture. Deployment will be limited by the number of situations in which a coal-power plant is located close enough to a geothermal resource. By contrast, water EGS must have adequate water resources nearby, and all of the water-EGS power is renewable geothermal power.

This page intentionally blank.

5 EXPLORATION

There are three important stages to developing and operating a geothermal power facility. They include field exploration, field development, and finally, site operation. Ultimately, wells need to be drilled into a geothermal resource before a geofluid can be brought to the surface to produce power. However, drilling wells at a potential geothermal site is a very expensive undertaking and as such a geothermal developer must be convinced that a viable fluid resource is present before starting. In fact, it has been estimated that the exploration stage can comprise as much as 42% of overall project costs [Jennejohn, 2009]. Hence, exploration procedures have evolved to increase the success rate in developing geothermal resources. Such procedures can be divided into two critical groups: predrilling and drilling. In the predrilling stage, remote sensing, geochemical, and geophysical surveys are conducted on promising locations for assessing the presence and viability of potentially productive and cost-effective geothermal resources. A detailed discussion of the specific methods employed in each of these surveys is beyond the scope of this study, but a good overview of them can be found elsewhere [USDOE, 2010].

Despite their cost impacts, predrilling methods have a negligible impact on the total life-cycle geothermal power, because they are mostly analytical in nature. Nonetheless, a brief discussion of them is in order. Before land access rights are obtained, remote sensing technologies such as satellite, airborne hyperspectral, and light detection and ranging methods are employed to indicate the presence of a resource. If a promising resource appears to be present, land rights are obtained and a series of geochemical (CO_2 and Hg concentrations of fluids, elemental and isotopic ratios, temperature gradients, others) and geophysical (magnetotellurics, resistivity, gravity, seismic tomography, others) measurements are conducted. If the results from these surveys are sufficiently encouraging, a decision is made to drill exploratory wells.

Unfortunately, little to no published information is available on the number of exploration wells needed to confirm the viability of the geofluid resource. Average drilling success rates and associated ranges would be very useful for our life-cycle assessments of geothermal power production. Sanyal and Morrow [2011] published a study on drilling success rates in the development and operational stages of existing geothermal fields, but unfortunately concluded that there is little information to establish success rates for the exploration stage. The two locations addressed in their study were the Geysers and Kamojang steam fields.

In our earlier analysis of geothermal power production [Sullivan et al., 2010, 2011], we estimated the life-cycle burdens of the exploration phase of well-field development as one additional production well. Admittedly, this is an approximation, but a necessary one due to the dearth of information on how the exploration drilling phase of geothermal well-field development is actually conducted. Further, this assumption implies that exploration wells have the same material requirements as production wells (and injection wells in the cases of EGS and HT-B plants). Generally, this is not the case. Exploration drilling is a combination of core holes, slim holes, thermal gradient holes, and finally confirmation wells. From a material-demand point of view, only the last of these can be equated to a production well. Hence, exploration wells are typically lower in material and fuel demand than production and injection wells, but our having

assumed their equivalence provided a more conservative estimate of exploratory well burden, especially given the uncertainty about the number of such wells needed to confirm a site's resource potential. In that study [Sullivan et al, 2010, 2011], the incremental cement, steel, and diesel fuel for the HT-B plant turned out to be about 22% of the existing burden for the production and injection wells. On the other hand, for the HT-F plant, the incremental burden was about 4.5%. The reason for the distinct difference between the two plants is related to plant capacity. In general, as capacity increases the number of wells required to support it is greater, although the number of exploration wells in both cases was assumed to be one. The ratio of exploration to production/injection wells was 1:4.1 for the HT-B plant and 1:20.6 for the HT-F plant.

To develop better estimates of the life-cycle burdens for the exploration stage of geothermal power, we have developed the following alternative approach. It is an approach inferred from industry input to the Geothermal Technologies Program (GTP) levelized cost of electricity (LCOE) initiative. The scheme is:

1. Using a variety of geochemical and geophysical assessments, assess up to five sites with some potential.
    a. From these sites, identify the three with the most potential.
    b. Drill five shallow and two deep core holes at each site.

2. From this set of sites, choose the one with the highest potential.

3. At this site, drill a series of confirmation wells (assumed here to be production wells).
    a. Site is declared a success if three out of no more than five confirmation wells are productive. A probability of success is attached to each confirmation well drilled.

For clarification purposes, we divide exploration into two stages: coring and confirmation.

We used this model to estimate life-cycle burdens of exploration drilling for EGS, HT-B, and HT-F facilities. EGS and HT-B are typically hidden resources (not evident at the surface), whereas for HT-F there are usually surface manifestations (fumaroles, mud pots, geysers, others). We define a successful site after Sanyal and Morrow [2011] as one where geofluid flow rate and temperature from its wells are sufficient to cost effectively meet the desired plant power output. Drilling wells is a very expensive proposition; and hence, companies developing geothermal technologies (GT) sites must be reasonably certain that a profitably exploitable resource is present and accessible. Toward that end, five shallow and two deep core (slim) holes are drilled at the three sites. For the purposes of our LCA, we treat core and slim holes as the same.

Boring these holes is much less expensive than drilling production wells. From those wells, the developer identifies two important findings: (1) the site with the most potential (highest resource temperature and potential flow rates) and (2) the subsurface distribution of the resource at the site. The latter informs the developer where it is best to drill confirmation wells at

the site with the most potential. While thermal gradient holes are also used by field developers, they are not considered here because they are typically narrow holes often drilled from the back of a truck, and hence, have negligible life-cycle footprints.

Because there is no guarantee of success even after core-hole surveying, a probability (P_1) is introduced to estimate the success rate for a confirmation well. Further, due to cost considerations, there is a limit on the amount of drilling a developer is willing to do to ascertain a site's viability; in our treatment, the maximum is assumed to be, at most, five confirmation wells. Overall, our model assumes that the amount of exploration drilling is independent of the output capacity of the final geothermal facility. Per successful facility, the scheme listed above amounts to 15 shallow core holes, six deep core holes, and on average about two to four confirmation wells, depending on P_1.

Based on the research of others [Jennejohn, 2009; Benoit et al.], we make the following core-hole assumptions: (1) a 6.75-in. core hole is bored to a depth of 0.25 in. of total well depth, which is subsequently cased with a 4.5-in. casing and cemented in place; and (2) from there, a 3.83-in. core hole is bored the rest of the way to the targeted depth. For our analysis, cement and casing materials are assigned to the hole/well as they are permanently attached. Also attributed are the water and diesel fuel required to drill the well or hole from the surface to the bottom. Core rods are not allocated to the well, because they are assumed to be reusable. Further, it was assumed that the shallow holes are drilled to one-half resource depth, whereas deep holes go all the way to the resource. We further assumed that the holes are cased to one-quarter of well depth. Confirmation wells are, in practice, intended to be production wells; the materials required for their construction have been discussed previously [Sullivan et al., 2010, 2011]. Because confirmation drilling in our model has a statistical component, the sum of the average number of failed confirmation wells on a successful site plus the average number of successful wells on failed sites, plus or minus one standard deviation, is attributed to the successful site. On the other hand, successful confirmation wells on a successful site are considered production wells; and hence, attributed to well-field development and not exploration.

The diesel fuel requirement is based on the daily fuel consumption rate for a 300 hp drilling rig (200 gallons/day) times the number of days required to drill the core holes. Based on Benoit et al. [2012] we assume that value to be about 34 days per km depth. Water consumption for core drilling is required in two places: (1) water for the cement in the cased zone of the core hole and (2) mud needed for cooling the coring tool and for flushing cuttings away. Based on industry practice for drilling rotary cone bits, the mud, and hence water requirements, are typically about five times the volume of the well/bore hole. Due to the hollow structure of core bits, we assumed the mud requirements to be five times the volume of the hole minus the core.

It is expected that the well field exploration (coring and confirmation) process adds materials, water, and diesel fuel to the overall life cycle for these facilities. The question is how much. Results from the model are shown in Figures 8 and 9. As seen in these figures, exploration activities do contribute appreciably to well field MPRs. In fact, for the EGS facility, the added steel and cement for exploration correspond to about 28% of their respective well-field MPRs. Exploration diesel is about 45% of the diesel MPR. These percentages (not absolute amounts)

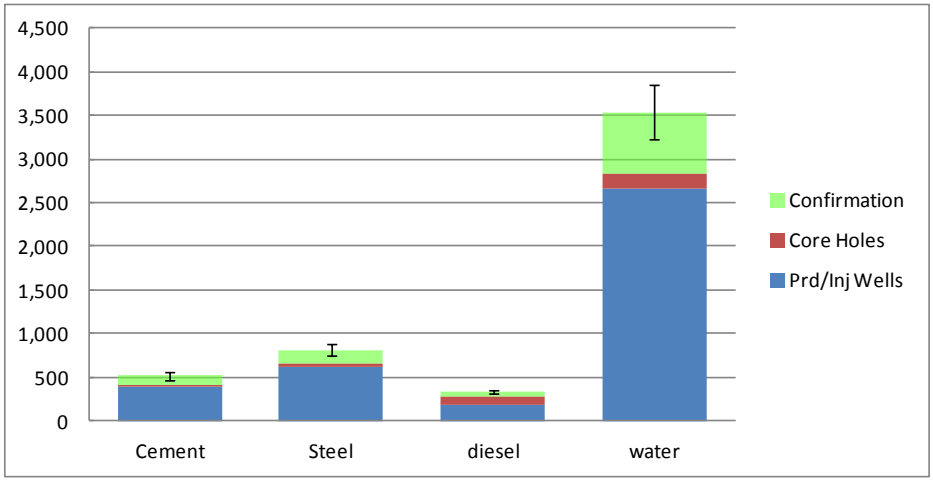

FIGURE 8 MPRs for 20 MW EGS plant wells including 5 km production and injection wells, core and slim hole exploration, and confirmation wells; units are mt/MW for steel and cement, and kL/MW for water and diesel fuel; error bars are ±1 stdev for confirmation wells.

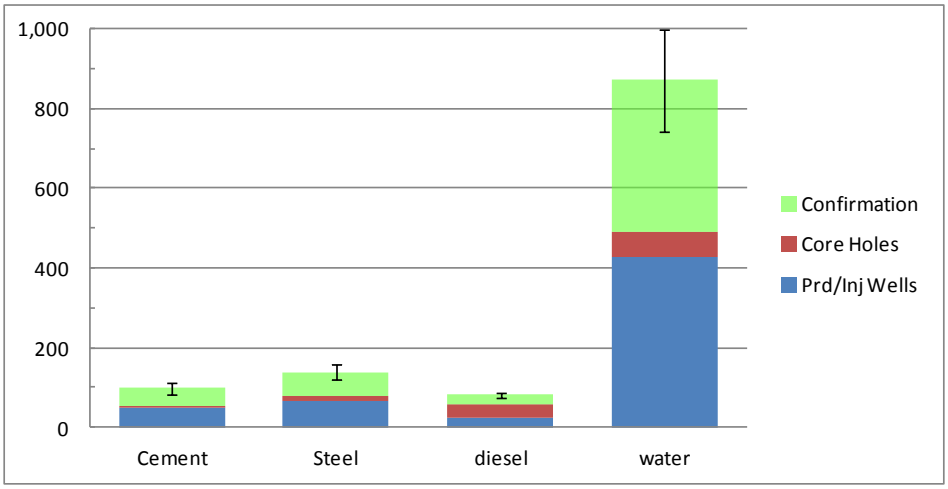

FIGURE 9 MPRs for a 10-MW HT-B plant well including 1-km production and injection wells, core and slim hole exploration, and confirmation wells; units are mt/MW for steel and cement, and kL/MW for water and diesel fuel; errors bars are ± 1 stdev for confirmation wells.

are independent of well depth. On the other hand, exploration water consumption is only about 14% of total well-field water consumption. This value is as low as it is due to well field stimulation, a process that is unique to EGS and typically requires large amounts of water. In this case, water for stimulation is about 7,800 kL/MW, which is 50% of the well-field water MPR.

The exploration percentages of well-field MPRs increase with decreasing facility capacity. For example, the percentages of well exploration cement, steel, and water MPRs for a 10-MW HT-B plant range from 46% to 50%. Due to the absence of well-field stimulation, the

percentage of exploration water to its total well-field MPR is sensibly the same as those for steel and cement. For diesel the percentage is about 68%. These values, all higher than those given above for the 20-MW EGS plant, are expected. Because exploration is a one-time activity with a fixed burden employed to identify a geothermal resource, the greater the output of a resource usually indicates more wells, which in turn diminishes the relative contribution of exploration to the overall life-cycle burden of the facility. In fact, if we apply our exploration model to a 50-MW HT-F facility, exploration well-field cement, steel, and water amount to about 15% of their respective well-field MPRs. However, the application of our model to HT-F facilities, which are generally sited where resources are conspicuous, might overestimate exploration life-cycle burdens somewhat.

With the exception of diesel, three-quarters or more of well-field exploration cement, steel, and water burdens are attributable to confirmation well drilling. It is roughly opposite for diesel consumption, which is mostly employed during coring activities.

For the above set of estimates, we assumed that the success rate for confirmation wells drilling is 60%. If instead a success rate of $P_1 = 80\%$ is assumed, the exploration component of the MPRs is markedly reduced. For the 10-MW HT-B plant, the exploration component of well-field cement, steel, and water MPRs ranges from 25% to 30%, and for diesel 60%, respectively, instead of the values given above. These values are markedly lower than the values cited above for this plant.

The variations (range bars) shown in Figures 8 and 9 are derived solely from the confirmation well drilling stage. They are due to failed wells on successful sites plus successful wells on unsuccessful sites during confirmation drilling. For $P_1 = 60\%$, they are roughly a third of the total exploration MPRs for water, cement, and steel; however, it is about 15% for diesel fuel.

We have not conducted an estimate of exploration for GPGE operations. In the case of green field sites, it would be consistent with natural gas exploration, about which we have no information. For reworked sites, the resource has already been developed, albeit degraded by increased brine (geofluid) and reduced gas production. Hence, for the latter, little if any additional exploration is expected.

Figures 10 and 11 show $\mathcal{E}_{pc}$ and GHG_{pc} values for the geothermal power systems covered herein. These plant cycle values were computed using cement, steel, diesel, and other materials employed for exploration, confirmation, production, and injection well drilling, plant construction and materials, and aboveground piping between wells and plants. As expected, the figures show increasing values of $\mathcal{E}_{pc}$ and GHG_{pc} with well depth. Further, notice that $\mathcal{E}_{pc}$ and GHG_{pc} values for EGS systems are considerably larger than are those of the HT-F plants. There are two reasons for this result: (1) very large air-cooling structures required for binary plant condensers comprise about half of the plant's steel and concrete; and (2) large amounts of cement, steel, and fuel are needed for drilling deep wells. Notice also that $\mathcal{E}_{pc}$ and GHG_{pc} for the HT-B plant are intermediate to those of EGS and HT-F technologies. This result is also expected. The HT-B system also uses air-cooling systems, but at the same time, its wells are much shallower than those used in the EGS technology. Finally, HT-F has the lowest $\mathcal{E}_{pc}$ and GHG_{pc}

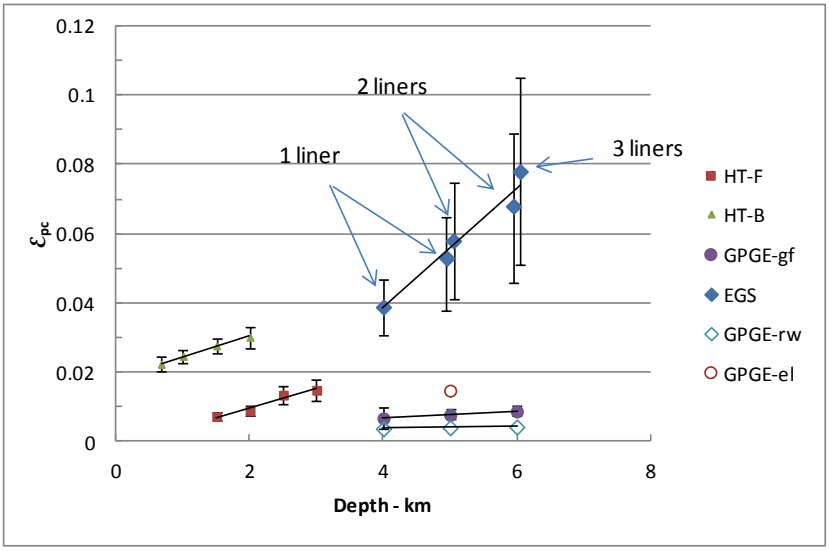

FIGURE 10 Plant cycle energy ratio for several geothermal energy technologies; range bars represent 1 standard deviation for EGS, HT-f, and HT-B; P_1=0.6.

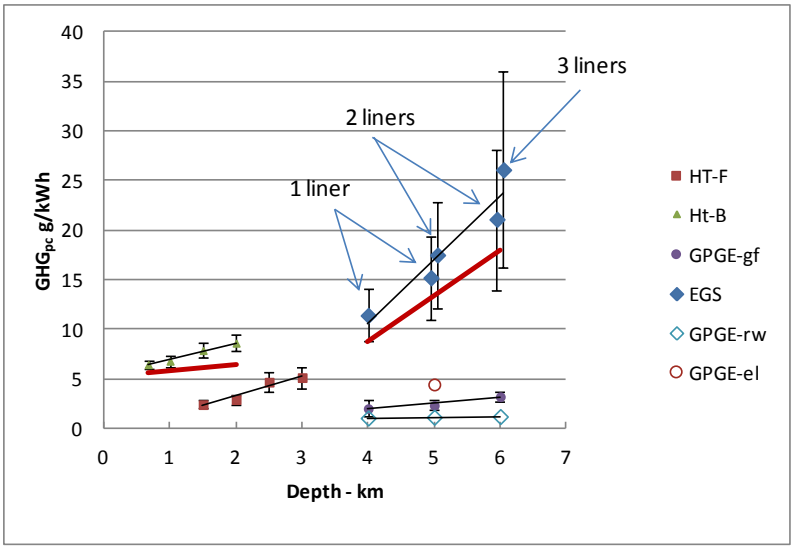

FIGURE 11 Plant cycle GHGs for several geothermal energy technologies; range bars represent 1 standard deviation for EGS, HT-f, and HT-B; solid red lines are for plants under the previous exploration scenario; P_1=0.6.

values for power-only geothermal technologies. These systems typically use water cooling, which requires smaller structures than air coolers, and have comparatively high-power output due to generally higher resource temperatures.

The range bars shown in Figures 10 and 11 arise from two effects: (1) variation in exploration drilling as discussed above and (2) run-to-run differences in the number of wells

required to meet design output power. The latter effect is a result of assumed variations in resource temperature, flow rates, the ratio of production to injection wells, and in the case of EGS, the use of submersible pumps at the highest flow rates. From the lowest to highest well depths, the magnitudes of the ranges are 24% to 38% for EGS, 16% to 21% for HT-F, and 7% to 10% for HT-B. Because the quantities plotted in Figures 10 and 11 are dependent on fixed terms and a well-depth-dependent variable term, the plots demonstrate a decreasing percentage of variation with decreasing well depth. In short, as well depth decreases, topside plant structures and plant-to-well piping energy and emissions (the fixed term) increase their magnitude relative to the well (variable) term.

The solid red lines seen in Figure 11 are trend lines from the previous [Sullivan et al., 2011] assessment of GHG_{pc} for our geothermal scenarios, where exploration was treated as one additional production well. Clearly, our current assessment shows a greater impact of exploration on GHG_{pc}. In fact, the differences between "old" and "new" trend lines range from 25% to 30% for EGS and 14% to 30% for HT-B. We don't show a previous trend line for HT-F, because it is virtually on top of the current trend line, which is not unexpected. Because the HT-F facility has a 50-MW capacity and over 20 wells, its exploration stage as is treated herein is a comparatively small part of the overall GHG_{pc}.

The drilling scheme employed in our model may not be representative of all exploration cases, but it is a method based on a systematic approach that was used by one developer. Although some developers may not conduct all the drilling employed in our model, there is a good chance that they will use information based on drilling conducted by a different entity; as far as our LCA is concerned, it is appropriate to include all data used to bring the power plant into operation, irrespective of when the data was gathered or by whom. Geothermal exploration drilling is widely viewed [Jennejohn, 2009; Fleischmann, 2006] as a very expensive and risky undertaking, and as such, considerable preliminary drilling is necessary before committing to full-scale development (drilling) of any potential well field.

This page intentionally blank.

6 GHG AND CRITERIA POLLUTANT EMISSIONS FROM POWER PRODUCTION

The generation of electricity in the United States is mostly derived from the combustion of fossil fuels. In the process of combustion, fossil fuels are consumed, fossil CO_2 is emitted, and other emissions such as CH_4, N_2O, NO_x, SO_x, PM_{10}, $PM_{2.5}$, VOCs, and CO are also emitted. The first two of these emissions are GHGs, whereas the last six are criteria air pollutants henceforth denoted as (CAP). These are controlled emissions that are managed to meet air emission regulations by emission control and abatement systems added onto power plants. The overall emissions generated during electricity production are substantial and driven by increasing demand for heat, light, and power for machinery, and could potentially grow considerably when electrically powered vehicles begin to penetrate the vehicle marketplace. Almost 40% of the primary energy in the United States is consumed by the electricity generating industry, and about 70% of that is derived from fossil fuels [EIA, 2010].

The GREET model, developed by Argonne National Laboratory [GREET 1, 2012; Wang 1999], includes electricity generation for a wide range of generating technologies burning various fuels. The model includes the energy and emission factors for GHG and CAP for each technology and fuel combination. These emission factors, expressed as g/kWh, are important upstream parameters for estimating life-cycle emissions associated with consumption of electric power for stationary and transportation applications. In 2012, Argonne released an important update [Cai et al., 2012] on power plant emission factors, which has been integrated into the most recent version of GREET 1 [2012].

The study by Cai et al. [2012] was a comprehensive effort that provided revised emission factors for a wide range of power generating technologies burning various fuels. While a detailed discussion of that work is beyond the scope of this study, a brief overview of their approach is merited.

Emission factors were developed for power derived from combustion of four main fuels: coal, natural gas, oil, and biofuels. Data were extracted from a number of sources including the U.S. Environmental Protection Agency's (EPA's) [2011] eGRID, EIA 923 [2007], and others. The focus of the update was primarily on emissions derived from power plant fuel consumption and not upstream emissions associated with fuel production or emissions associated with the plant cycle. While most plants burn only one fuel, a few burn more than one and were taken into consideration on a fuel/power technology basis. Some plants provided a combination of heat and power. They were not included due to issues around allocation of burdens to each energy output (i.e., heat and power). Plant energy conversion efficiencies (on a low heat value basis), technology distributions, and fuel composition (e.g., carbon and sulphur content) were considered from which emissions factors were developed on both a national and a state-by-state basis.

A statistical analysis was also conducted. On the basis of the updated GHG and CAP emission factors and energy efficiencies for the various power technologies by fuel type, the probability distribution functions were developed to describe the relative likelihood for the

emission factors and energy efficiencies as a function fuel type and generating technology. This was done on a national average basis.

Also recently added to GREET1 [2012] were plant cycle energy and GHG and CAP emissions for the various power generating technologies: fossil and renewable. Included in this addition were energy and emissions for three geothermal technologies, namely EGS, HT-B, and HT-F. Plant cycle additions to GREET were based on the LCAs conducted previously [Sullivan et al., 2010, 2012] for the geothermal effort.

Figure 12 (values in Table A-1, Appendix A) summarizes, by life-cycle stage, our life-cycle GHG emissions estimates (in g/kWh) for the various power technologies considered herein. The values shown in Figure 12 are averages. Figure 12 is consistent with our previous conclusions [Sullivan et al., 2010]. The strictly fossil fuel plants generate much more GHGs per kilowatt-hour than their renewable, hybrid, and nuclear counterparts. As expected, IGCC power has lower GHG emissions than its conventional thermoelectric counterparts for coal and biomass. This is a consequence of the greater efficiency of IGCC technologies. For the fossil electricity plants, the preponderance of GHG arises from the fuel burned to produce the electricity.

All plants shown in Figure 12 have GHG emissions in one or more of the stages in their life cycles. For example, all plants have emissions in their plant cycle stage, although for many

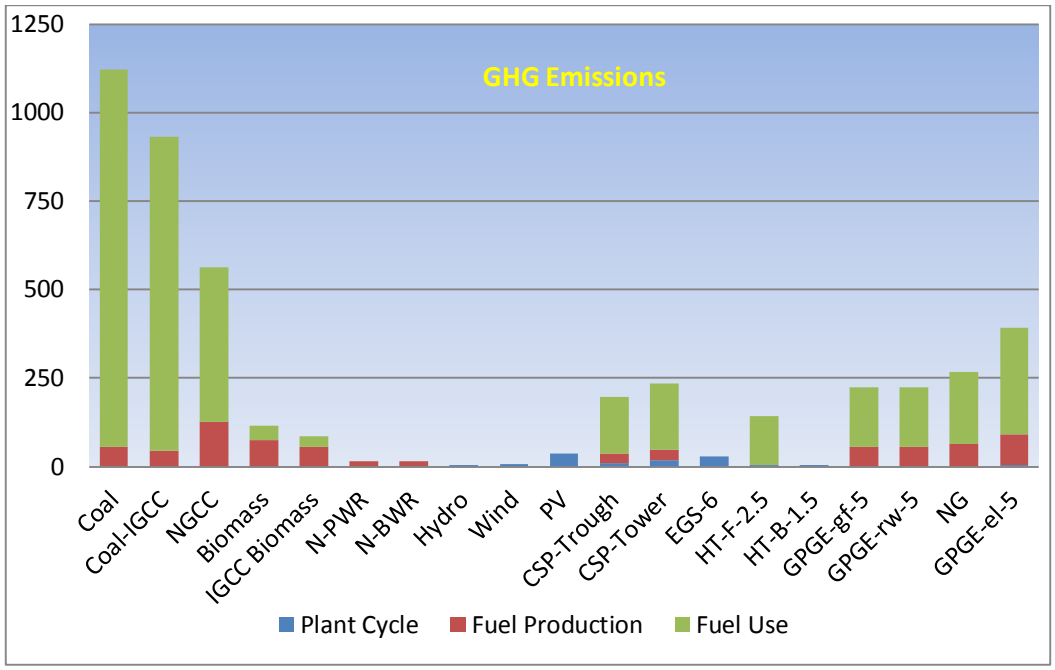

FIGURE 12 GHG emissions (g/kWh) by life-cycle stage for various power production technologies relative to total energy output (electricity and/or natural gas); entries are based on average MPRs given above and GREET1_2012 data; numerical postscripts denote well depths in km.

of them this is not conspicuous in the figure. Further, GHGs are emitted during the fuel production stage for fossil, biomass, nuclear, and the hybrid technologies, and during the fuel use stage for fossil, hybrids, biomass, and HT-F. The percentage of renewable energy output for the hybrid technologies was assumed to be 85% for CSP, 17% for GPGE-rw and GPGE-gf, and 31% for GPGE-el; the balance in each case was fossil-based electricity.

Among the renewable technologies shown in Figure 12, hydro, wind, PV, EGS and HT-B have the lowest GHG emissions, whereas HT-F and biomass power have the highest. In either case, they are considerably lower than those from the strictly fossil fueled power plants. For HT-F, the GHGs are, as discussed above, fuel-use emissions, which come primarily from dissolved CO_2 in the geofluid that is released to the atmosphere upon its passage through the plant. GHGs are emitted during biomass production and use, and arise from fuel use in harvesting forestry residues and incomplete combustion at the power plant yielding methane and nitrous oxide (N_2O) emissions during fuel use. The hybrid plants (GPGE and CSP) have higher GHG emission rates than those from the renewable technologies, though still considerably lower than those from strictly fossil fueled plants. This is a consequence of their dual output, one fossil (natural gas) and the other renewable (geofluid power). Due to comparatively minor material and fuel requirements for reworking a GPGE site or drilling a new green field site, their GHG values are sensibly the same.

For comparison purposes, a natural gas (NG) production and use bar (from GREET1_2012) has been added to Figure 12, representing the production of solely natural gas from associated wells and its combustion in a utility/industrial boiler. When this bar is compared to those for the GPGE-gf and GPGE-rw dual-output systems (gas and electricity), it is seen to be conspicuously higher because its lacks the leveraging effect of the dual output GPGE plants. The electric-power component of the GPGE dual output emissions arises from the plant cycle stage and is very small (barely visible in the figure).

Despite its consumption of about twice the natural gas of simply producing and delivering a unit of natural gas to a consumer, the GHG emissions from the GPGE-el plant are only somewhat higher than those for natural gas production and delivery. This is due to geofluid-powered electricity production, which is about a third of the systems output. For the same reason, its GHG emissions are lower than those of a comparable NGCC plant.

CAP results generated from GREET1 [2012] for the various power generation technologies are shown in Figure 13. Because of the range of emission levels, the results are presented on a logarithmic scale. Though GREET1 reports both 2.5- and 10-micron PM, to reduce clutter, the plot shows only PM_{10} results. Data values are given in Table A-2 in Appendix A. From an inspection of the figure, it is clear that the strictly combustion-based electric power-generating technologies shown at the graph's left side, including biomass fueled technologies, overall generate one or more orders of magnitude more CAP emissions than those of nuclear and renewable technologies. The emissions from the GPGE facilities (on the right side of the figure) are only marginally lower than those from the strictly combustion-based plants. Although the dominant energy output from the GPGE dual output facilities is natural gas, its associated emissions relative to those for strictly natural gas production are weighted downward somewhat by its geothermal electricity output. On the other hand, when a GPGE-el facility is

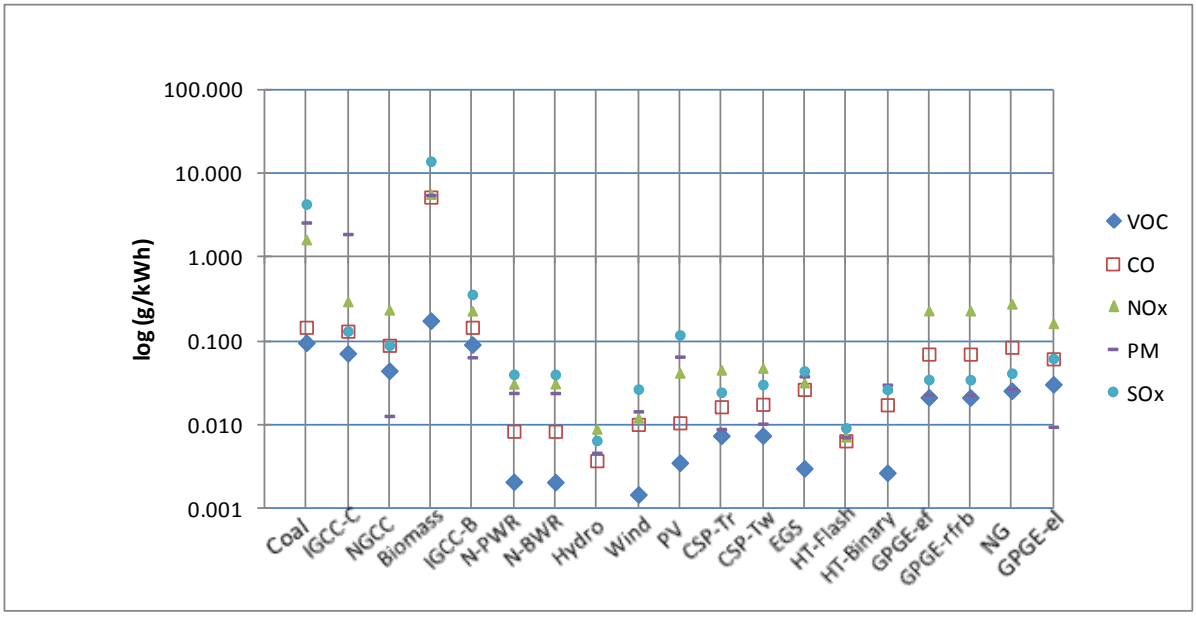

FIGURE 13 CAPs (g/kWh) over the life cycles of various power-production technologies.

compared to NGCC, its strictly fossil counterparts, its emission performance is somewhat better, again due to the leveraging effect of geothermal power output. However, overall, emissions from GPGE-rw, GPGE-gf, NG, and GPGE-el are quite similar.

With the exception of coal and biomass boiler power, on balance SO_x emissions for the rest of the technologies are roughly 0.032 g/kWh. The comparatively high SO_x values for coal are related to sulphur contents of the fuels. As for biomass, the high concentration of sulphur emissions is a result of cofueling those plants with a high percentage of municipal solid waste and black liquor from the paper industry. Notice that their IGCC counterparts have much lower SO_x emissions. This is a consequence of IGCC technology where sulphur gases must be scrubbed from the synthesis gas before combustion. With the exception of SO_x emissions, PV life-cycle CAPs are in good accord with those of the other renewable technologies. PV's somewhat higher SO_x value is a consequence of plant cycle emissions associated with copper and silicon production.

VOCs are consistently below 0.01 g/kWh and NO_x emissions are below 0.1 g/kWh for the renewable and CSP technologies, although the latter, a hybrid technology, tends to be on the higher side of that grouping. On the other hand, VOC and NO_x emissions are considerably higher (sometimes by more than an order of magnitude) than combustion based technologies, which includes the GPGE scenarios for either dual gas and electric or all electric outputs. The CO emissions for the renewable and CSP technologies, as a group, range about 0.013 g/kWh and as such are conspicuously lower than those for the combustion based technologies, albeit a little less so for the GPGE set. While CSP technologies have been assumed to be hybrid technologies, their fossil profile is considerably lower when compared to GPGE and consequently their CAP emissions more closely resemble those of the renewable technologies. Finally, with the exception

of coal boiler, IGCC coal, and biomass boiler technologies, particulate emissions appear to range widely between 0.005 and 0.0065 g/kWh.

Overall, the GHG and CAP emissions are as expected: higher for combustion based power, intermediate for hybrid power, and lowest for renewable power. In the case of renewable technologies, their GHG and CAP emissions arise from the plant cycle only, a one-time charge of emissions (except for HT-F GHGs) over the plant lifetime. Results clearly show that GHG and CAP emissions from geothermal facilities are very much less than those from the strictly fossil-based technologies, lower than those from the hybrid technologies, and mixed for those of the renewable technologies. Among the geothermal technologies, HT-B has the lowest GHGs, on par with hydro and wind; EGS has midrange GHGs which are on par with PV; and HT-F has the highest, incurred during plant operation.

This page intentionally blank.

7 CONCLUSIONS

A number of important issues with geothermal power have been addressed. These topics included GHG emissions from hydrothermal flash and steam plants, use of supercritical CO_2 as a working fluid for EGS, the impact of geothermal field exploration on geothermal life cycles, and finally, GHGs and CAP emissions from a range of power plants including geothermal plants.

An analysis of California GHG emissions from geothermal plants was conducted using DOE power generation data to develop an emissions distribution function from flash and dry stream geothermal plants in California. From that analysis, it is found that the GHG emissions range from 11 to 370 g/kWh with a weighted average of 98 g/kWh. Hydrothermal binary plants were assumed to have zero GHG emissions. In our view, these results are a good preliminary estimate of California geothermal GHG emissions. Limitations of the currently available California GHG data, including incomplete reporting and the use of calculated versus measured values, were discussed as well as when new and better data might be released.

A model was developed to estimate the life-cycle burdens of geothermal systems (EGS) utilizing $scCO_2$ as a working fluid. The model represents a coupled hypothetical (CCS/EGS) system comprised of coal and EGS plants where captured CO_2 from the former is compressed and pumped via pipeline to the latter to serve as a makeup $scCO_2$ offsetting reservoir losses. These losses are considered to provide a sequestration mechanism for the coal plant. Upon adjusting the power output from a coal plant for carbon capture and combining it with EGS power output enabled by the $scCO_2$, net energy and emissions associated with the coupled system were computed. Relative to stand-alone CCS coal plants, the combined plant demonstrated substantial reductions in fossil energy consumption and atmospheric CO_2 emissions. The magnitude of these savings is dependent on the $scCO_2$ consumption rate and carbon capture efficiencies, the latter of which ranged from 0% to 90%. Also accounted for were reservoir leakage rates and concomitant atmospheric reductions of both prompt and leaked CO_2 due to repartitioning of the gas between the atmosphere, oceans, and biosphere. For example, a CCS/EGS plant operating for 30 years emits to the atmosphere 635 g per kWh produced after 100 years from startup, assuming a 1% leakage rate from the EGS $scCO_2$ reservoir. However, when atmospheric CO_2 attrition is accounted for, only 223 g per kWh produced remains in the atmosphere after 100 years.

The potential for sequestering a substantial fraction of coal power generated CO_2 emissions with $scCO_2$ EGS in the United States is likely limited because of the distributed nature of the existing coal plant infrastructure and the need for proximity to a geothermal resource. Nevertheless, $scCO_2$ EGS consumption of coal power CO_2 could provide an energy and emission value when fossil fuel power plants and geothermal resources coincide, cost permitting.

To compensate for a lack of quantitative information on the magnitude of exploration-well field drilling, a model was developed to improve our previous estimate for this stage's life-cycle burdens (i.e., one additional production well). The model is based on industry input about the extent of exploration drilling. It follows a scheme of drilling core holes on several sites, one of which is chosen for confirmation well drilling. A probability of success is attached for each

confirmation well drilled. Our new exploration estimates indicate a 25% to 30% increase in plant cycle GHG emissions for EGS, 14% to 30% for HT-B, and little change for HT-F over previous values. Exploration results are dependent on well depth. Although the magnitudes of required materials and fuel for well-field exploration are dependent on well depth, they are for the most part independent of well depth when viewed on a basis relative to total well field development.

Finally, an analysis was conducted on the overall GHG and CAP emission from a wide range of power generation technologies including fossil, renewable, and hybrid (combined fossil and renewable). As expected, emissions from the strictly renewable technologies are one to one and a half orders of magnitude less than those from the fossil plants. On the other hand, the hybrid plants, which produce both fossil and renewable energy, only emit about a half an order of magnitude less than their fossil counterparts. Overall, renewable plants have the fewest emissions. GHG and CAP emissions from geothermal facilities are small and arise primarily from the plant cycle, although flash plants have some GHG emissions during the operational stage. The hybrid plants emit roughly 40% to 60% more GHGs than the hydrothermal flash/steam plants assuming the U.S. average GHG emission for the latter.

REFERENCES

Benoit, D., J. Moore, and C. Goranson. "Core Hole Testing and Drilling at the Lake City, California Geothermal Field." Accessed April 30, 2012. https://pangea.stanford.edu/groups/warners/PDFs/Core%20Hole%20Drilling.pdf.

Bertani, R., and I. Thain. 2001. "Geothermal Power Generating Plant CO_2 Emission Survey, Rev. 1.0, International Geothermal Association." Accessed August 2010. http://www.jeotermaldernegi.org.tr/ian%20i.htm.

Bloomfield, K.K., J.N. Moore, and R.M. Neilson, Jr. 2003. "Geothermal Energy Reduces Greenhouse Gases," *Climate Change Research*, March/April: 77–79.

Brown, D.W. 2000. A Hot Dry Rock Geothermal Energy Concept Utilizing Supercritical CO_2 Instead of Water, *Proceedings, Twenty-Fifth Workshop on Geothermal Reservoir Engineering*, Stanford, California, January 24–26 2000 SGP-TR-165 (Stanford, CA: Stanford University).

Cai, H., M.Q. Wang, A. Elgowainy, and J. Han. 2012. Updated Greenhouse Gas and Criteria Air Pollutant Emission Factors and Their Probability Distribution Functions for Electric Generating Units, ANL/ESD/12-2.

CEPA (California Environmental Protection Agency). 2010. Air Resources Board, Reported Emissions, Facility Emissions. Accessed August 16, 2011. http://www.arb.ca.gov/cc/reporting/ghg-rep/ghg-rep.htm.

Ciferno, J. 2006. CO_2 Capture from Existing Coal-Fired Power Plants. Accessed February 3, 2012. http://www.netl.doe.gov/energy-analyses/pubs/CO2%20Retrofit%20From%20Existing%20Plants%20Revised%20November%202007.pdf.

Clark, C.E., C.B. Harto, , J.L. Sullivan, , and M.Q. Wang. 2011a. *Water Use in the Development and Operation of Geothermal Power Plants,* ANL/EVS/R-10/5.

Clark, C.E., C.B. Harto, and W.A. Troppe. 2011. Water Resource Assessment of Geothermal Resources and Water Use in Geopressured Resources, ANL/EVS/R-11/10.

Doctor, R. 2011. Economic Comparison of CO_2 Capture and Sequestration from Amines and Oxyfuels. Report to Environmental Projects Division, U.S. Department of Energy, National Energy Technology Laboratory. December 29, 2011. Morgantown.

Dunn, P. 2010. Baseline System Costs for 50.0 MW Enhanced Geothermal System. *GSPAWG Meeting, November 17–18, 2010* (Washington, D.C.: Department of Energy).

EIA (Energy Information Administration). 2010. *Annual Energy Outlook 2010*, Tables A8 and A16, http://search.usa.gov/search?affiliate=eia.doe.gov&v%3Aproject=firstgov&query=annual+energy+outlook+2010, Accessed August 2010.

EIA-923. 2010. Department of Energy, The Energy Information Administration (EIA), 2010, EIA-923 Monthly Time Series File, Sources EIA-923 and EIA-860. Accessed June 25, 2012. http://www.eia.gov/electricity/data/eia923/.

EPA. 2011a. The Emissions & Generation Resource Integrated Database (eGRID 2010 Version 1.1). Accessed March 2012. http://www.epa.gov/cleanenergy/energy-resources/egrid.

Fleischmann, D.J. 2006. Geothermal Resource Development Needs in Arizona, Geothermal Energy Association, GEA. Accessed 4/15/2012. http://geo-energy.org/plants.aspx.

Frank, E.D., J.L. Sullivan, and M.Q. Wang. 2012. Life Cycle Analysis of Geothermal Power Generation with Supercritical Carbon Dioxide, Environ., Res. Lett., 7, open access.

GEA, 2012, Geothermal Energy Association, Geothermal Plants, http://geo-energy.org/plants.aspx, Accessed 10/17/2012.

GREET1. 2012. Greenhouse Gases, Regulated Emissions and Energy in Transportation (GREET) model. Accessed July 31, 2012. http://greet.es.anl.gov/greet_1_series.

Hansen, J., M. Sate, P. Kharecha, G. Russell, D.W. Lea, and M. Siddall. 2007. Climate change and trace gases, *Phil. Trans. R. Soc.*, A, (365): 1925–1954.

Houghton, J.T. 1997. Global Warming, Cambridge University Press, Cambridge, UK.

Jennejohn, D. 2009. *Research and Development in Geothermal Exploration and Drilling*, Geothermal Energy Association, Washington, D.C.

Joos, F., I.C. Prentice, S. Sitch, R. Meyer, G. Hooss, G.K. Plattner, S. Gerber, and K. Hasselman. 2001. Global Warming Feedbacks on Terrestrial Carbon Uptake under Intergovernmental Panel on Climate Change (IPCC) Emission Scenarios, *Global Biogeochemical Cycles*, vol. 15(4), 891–907.

Mobley, R. 2011. Baseline System Costs for 50.0 MW Enhanced Geothermal System, GSPAWG Meeting, August 24, 2011. Washington, D.C.

Nelson, C.R., J.M. Evans, J.A. Sorensen, E.N. Steadman, and J.A. Harju. 2005. *Factors Affecting the Potential for CO_2 Leakage from Geological Sinks* (Grand Forks, ND: University of North Dakota). http://www.undeerc.org/PCOR/newsandpubs/pdf/FactorsAffectingPotential.pdf.

Pruess, K. and M. Azaroual. 2006. On the Feasibility of Using Supercritical CO_2 as Heat Transmission Fluid in an Engineered Hot Dry Rock Geothermal System, *Proceedings, Thirty-first Workshop on Geothermal Reservoir Engineering, Stanford University, Stanford, California, January 30–February 1, 2006 SGP-TR-179* (Stanford, CA: Stanford University).

Pruess, K. 2007. Enhanced Geothermal Systems (EGS): Comparing Water and CO_2 as Heat Transmission fluids *Proceedings, New Zealand Geothermal Workshop 2007, Auckland, New*

Zealand, November 19-21,2007 LBNL-63627 (Berkeley, CA: Lawrence Berkeley National Laboratory). http://www.osti.gov/bridge/product.biblio.jsp?query_id=5&page=0&osti_id =922829.

Remoroza, A.I., B. Moghtaderi, and E. Doroodchi. 2011. Coupled Wellbore and 3D Reservoir Simulation of a CO_2 EGS Proceedings, Thirty-Sixth Workshop on Geothermal Reservoir Engineering Stanford University, Stanford, California, January 31 – February 2, 2011 SGP-TR-191. (Stanford, CA: Stanford University).

Rule, B.M., Z.J. Worth, and C.A. Boyle, 2009, Comparison of Life Cycle Carbon Dioxide Emissions and Embodied Energy in Four Renewable Electricity Generation Technologies in New Zealand, *Environ. Sci. & Technol*., 43, 6406–6413.

Sanyal, S.K., and J.W. Morrow. 2011. An Investigation of Drilling Success in Geothermal Exploration, Development and Operation, GRC *Transactions*, vol. 35, 233–237.

Shine, K.P., J.S. Fuglestvedt, K. Hailemariam, and N. Stuber. 2005. Alternatives to the Global Warming Potential for Comparing Climate Impacts of Emissions of Greenhouse Gases, *Climate Change*, 68: 281–302.

Sullivan, J.L., C.E. Clark, J. Han, and M. Wang. 2010. Life-Cycle Analysis Results of Geothermal Systems in Comparison to Other Power Systems, ANL/ESD/10-5.

Sullivan, J.L., C.E. Clark, L. Yuan, J. Han, and M. Wang. 2011. *Life-Cycle Analysis Results of Geothermal Systems in Comparison to Other Power Systems*, Part II, ANL/ESD/11-12.

Tester J.W., B. Anderson, A. Batchelor, et al. 2006. The Future of Geothermal Energy: Impact of Enhanced Geothermal Systems (EGS) on the United States in the 21st Century. Final Report to the US Department of Energy Geothermal Technologies Program, Cambridge, MA: Massachusetts Institute of Technology.

USDOE (United States Department of Energy). 2010. *A History of Geothermal Energy Research and Development in the United States, 1976–2006, Volume 3: Reservoir Engineering*. Accessed March 16, 2011. http://www1.eere.energy.gov/geothermal/pdfs/zgeothermal_history_3_ engineering.pdf.

Wang, M. 1999. GREET 1.5—Transportation Fuel-Cycle Model, Vol. 1: Methodology, Use, and Results, Report No. ANL/ESD-39, Argonne National Laboratory.

This page intentionally blank.

APPENDIX A

TABLE A-1 GHG Emissions for a range power generation technologies at the wall outlet: all units are g/kWh$_{elec}$.

Life Cycle Stage	Coal	Coal IGCC	NGCC	Biomass	Bio-IGCC	Nuc-PWR	Nuc-BWR	Hydro	Wind	PV
Plant cycle	0.690	1.12	0.34	0.64	0.70	0.45	0.58	5.44	8.00	37.8
Fuel production	56.4	43.4	126	73.8	54.1	16.0	16.0	0.0	0.0	0.0
Fuel use	1064	888	436	40.6	31.5	0.0	0.0	0.0	0.0	0.0
Total	1121	932	563	115	86.3	16.5	16.6	5.4	8.0	35.8

TABLE A-1 (cont.) GHG emissions from various power generating technologies at the wall outlet: all units are g/kWh$_{all_outputs}$.

Emission	CSP–tr	CSP-tw	EGS	HT-F	HT-B	GPGE-gf	GPGR-rw	NG	GPGE-el
Plant cycle	10.6	17.9	27.7	4.10	5.73	2.32	1.11	0.00	4.39
Fuel production	25.8	29.8	0.0	0.0	0.0	53.8	53.8	65.0	87.1
Fuel use	161	186	0.0	140	0.0	168	168	203.0	300
Total	197	234	27.7	144	5.7	224.1	223	268	391

TABLE A-2 CAP Emissions for various power generation technologies at the wall outlet: all units are g/kWh$_{elec}$.

Emission	Coal	Coal IGCC	NGCC	Biomass	Bio-IGCC	Nuc-PWR	Nuc-BWR	Hydro	Wind	PV
VOC	0.095	0.071	0.044	0.174	0.090	0.002	0.002	0.000	0.001	0.004
CO	0.146	0.131	0.089	5.200	0.145	0.008	0.008	0.004	0.010	0.011
NO_x	1.617	0.295	0.235	5.631	0.229	0.031	0.031	0.009	0.012	0.042
PM_{10}	2.000	1.502	0.008	3.103	0.040	0.018	0.018	0.003	0.011	0.049
$PM_{2.5}$	0.585	0.381	0.005	2.400	0.024	0.006	0.006	0.001	0.004	0.016
SO_x	4.291	0.131	0.089	13.908	0.359	0.040	0.040	0.006	0.027	0.118
CH_4	1.583	1.302	3.505	0.689	0.088	0.044	0.044	0.004	0.026	0.063
N2O	0.0179	0.0407	0.0015	0.0812	0.1010	0.0002	0.0002	0.0000	0.0001	0.0005

TABLE A-2 (cont.) CAP emissions from various power generating technologies at the wall outlet: all units are g/kWh$_{all_outputs}$.

Emission	CSP–tr	CSP-tw	EGS	HT-F	HT-B	GPGE-gf	GPGR-rw	NG	GPGE-el
VOC	0.007	0.007	0.003	0.001	0.003	0.021	0.021	0.025	0.030
CO	0.016	0.018	0.026	0.006	0.017	0.070	0.070	0.084	0.061
NO_x	0.045	0.048	0.032	0.007	0.028	0.230	0.230	0.277	0.162
PM_{10}	0.006	0.008	0.027	0.005	0.020	0.012	0.012	0.014	0.006
$PM_{2.5}$	0.003	0.003	0.011	0.002	0.010	0.011	0.011	0.013	0.004
SO_x	0.024	0.030	0.044	0.009	0.026	0.035	0.034	0.041	0.062
CH_4	0.541	0.544	0.043	0.760	0.040	1.539	1.539	1.859	2.412
N_{2O}	0.0003	0.0003	0.0002	0.0000	0.0002	0.0034	0.0034	0.0041	0.0011

Energy Systems Division
Argonne National Laboratory
9700 South Cass Avenue, Bldg. 362
Argonne, IL 60439-4815

www.anl.gov